

# Data-driven integration of hippocampal CA1 synapse physiology in silico

András Ecker<sup>1\*</sup>, Armando Romani<sup>1</sup>, Sára Sárany<sup>2,3</sup>, Szabolcs Káli<sup>2,3</sup>, Michele Migliore<sup>4</sup>, Audrey Mercer<sup>5</sup>, Henry Markram<sup>1</sup>, Eilif Muller<sup>1</sup>, and Srikanth Ramaswamy<sup>1\*</sup>

<sup>1</sup>*Blue Brain Project, École polytechnique fédérale de Lausanne, Campus Biotech, Geneva, Switzerland*

<sup>2</sup>*Institute of Experimental Medicine, Hungarian Academy of Sciences, Budapest, Hungary*

<sup>3</sup>*Pázmány Péter Catholic University, Faculty of Information Technology and Bionics, Budapest, Hungary*

<sup>4</sup>*Institute of Biophysics, National Research Council, Palermo, Italy*

<sup>5</sup>*UCL School of Pharmacy, University College London, London, United Kingdom*

\*Correspondence: [andras.ecker@epfl.ch](mailto:andras.ecker@epfl.ch), [srikanth.ramaswamy@epfl.ch](mailto:srikanth.ramaswamy@epfl.ch)

## 1 Abstract

2 The anatomy and physiology of synaptic connections in rodent hippocampal CA1 have been  
3 exhaustively characterized in recent decades. Yet, the resulting knowledge remains disparate  
4 and difficult to reconcile. Here, we present a data-driven approach to integrate the current  
5 state-of-the-art knowledge on the synaptic anatomy and physiology of rodent hippocampal CA1,  
6 including axo-dendritic innervation patterns, number of synapses per connection, quantal con-  
7 ductances, neurotransmitter release probability, and short-term plasticity into a single coherent  
8 resource. First, we undertook an extensive literature review of paired-recordings of hippocam-  
9 pal neurons and compiled experimental data on their synaptic anatomy and physiology. The  
10 data collected in this manner is sparse and inhomogeneous due to the diversity of experimental  
11 techniques used by different labs, which necessitates the need for an integrative framework to  
12 unify these data. To this end, we extended a previously developed workflow for the neocortex to  
13 constrain a unifying *in silico* reconstruction of the synaptic physiology of CA1 connections. Our  
14 work identifies gaps in the existing knowledge and provides a complementary resource towards  
15 a more complete quantification of synaptic anatomy and physiology in the rodent hippocampal  
16 CA1 region.

17

18 **Keywords:** hippocampus, data integration, in silico modeling, CA1, synapse

## 19 1 Introduction

20 The hippocampal CA1 region is probably the most studied region of the mammalian brain and  
21 is thought to play a pivotal role in learning and memory ([Bliss and Collingridge, 2013](#); [Buzsáki, 1989](#)).  
22 Neuronal microcircuits in the hippocampal CA1 region process and store information  
23 through a myriad of cell-type-specific synaptic connections. Previous studies have identified that  
24 hippocampal cell-types are connected through multiple synapses, which are positioned across  
25 distinct axo-dendritic domains with a diversity of short- and long-term dynamics, as well as  
26 synaptic strengths. Despite the wealth of data, we lack an integrative framework to reconcile the  
27 diversity of synaptic physiology, and therefore, identify knowledge gaps. There have been several

28 recent attempts to integrate knowledge about the hippocampal CA1 (Bezaire and Soltesz, 2013;  
29 Wheeler et al., 2015), however, they were not focused on the dynamics of synaptic transmission.  
30 Recent attempts have extended the utility of the online resource hippocampome.org towards  
31 synaptic electrophysiology as well (Moradi and Ascoli, 2019). However, in the continuing spirit  
32 of hippocampome.org, the study is primarily a text mining-based collection of papers and pa-  
33 rameters, which does not integrate these data into a unifying framework. As a way forward,  
34 we extended a previously developed workflow to integrate disparate data on the physiology of  
35 synaptic transmission in hippocampal CA1, identified and extrapolated organizing principles to  
36 predict knowledge gaps (Markram et al., 2015). We accounted for the dynamic and probabilistic  
37 nature of synaptic transmission by fitting experimental traces using a stochastic generalization of  
38 the Tsodyks-Markram short-term plasticity model (Tsodyks and Markram, 1997; Markram et al.,  
39 1998; Fuhrmann et al., 2002). After validating the number and location of synapses, parame-  
40 terizing the release probability and reversal potentials, as well as depression, facilitation, and  
41 synaptic conductance rise and decay time constant for various hippocampal connection types,  
42 we corrected for space clamp artefacts in silico by tuning synaptic conductance to match the in  
43 vitro PSP (postsynaptic potential) amplitudes. We also considered temperature and extracellu-  
44 lar calcium concentration ( $[Ca^{2+}]_o$ ) differences, which were adjusted using Q10 and Hill scaling  
45 factors, respectively. The resulting models for a subset of hippocampal connection types were  
46 applied predictively to the remaining uncharacterized connection types by clustering them into  
47 nine groups based on synapse types and neuronal biomarkers and applying the known param-  
48 eters within each group. Curated and predicted parameters presented here should serve as a  
49 resource to researchers aiming to model hippocampal synapses at any level, while the detailed  
50 methodology intends to give a guideline to utilize such a framework to integrate data from other  
51 brain regions or species.

## 52 2 Methods

### 53 2.1 Circuit building and synapse anatomy

54 A detailed model of the rat hippocampal CA1 area was built using the pipeline of Markram et al.  
55 (2015). Circuit building and rigorous validation will be detailed in a following article. In brief,  
56 single cell models with detailed morphologies including axonal reconstructions from Migliore  
57 et al. (2018) were populated in an atlas-based volume corresponding to the dimensions of the  
58 hippocampal CA1 region. Structural appositions between axons and dendrites were detected  
59 based on touch distance criteria and were later pruned to match experimentally reported bouton  
60 density, number of synapses per connections and connection probability using an algorithm to  
61 yield the functional connectome (Reimann et al., 2015). In this manner, the number and location  
62 of synapses for each connection were constrained in a data-driven manner. Connected cell-types  
63 were sampled from this circuit based on their inter-somatic distance.

### 64 2.2 Dendritic features of single cell models

65 Detailed biophysical models of pyramidal cells (PCs) and interneurons of the CA1 region from  
66 Migliore et al. (2018) were re-optimized and used in the present study. All models were con-  
67 strained with active dendritic conductances but were optimized using only somatic features  
68 (Migliore et al., 2018). While the somatic responses to various step-current injections were cor-  
69 rect, the dendrites of the single cell models turned out to be too excitable (single synaptic input  
70 leading to spikelets and somatic spikes). For this reason, single cell models were re-optimized  
71 with slightly reduced range for dendritic sodium channel density. PSP propagation and atten-  
72 uation along the dendritic branches is a key feature for our synaptic conductance calibration,

73 thus it was validated against experimental data using the HippoUnit framework (unpublished).  
74 To this end, excitatory postsynaptic current (EPSC) like currents were injected into the apical  
75 trunk of PCs with varying distance from the soma and PSPs were simultaneously measured at  
76 the local site of the injection and in the soma.

### 77 **2.3 Correcting for calcium ion concentration, temperature and liquid junction potential** 78

79 Published parameters from different sources were corrected for differences arising from distinct  
80 experimental protocols. This included corrections for extracellular calcium levels different from 2  
81 mM, temperatures different from 34 °C and liquid junction potential (LJP) in the case of whole-  
82 cell recordings using patch pipettes. The correction for  $[Ca^{2+}]_o$  was done by scaling the  $U_{SE}$   
83 parameter of the synapses (see below), using the Hill isotherm with  $n = 4$  (Hill, 1910):

$$U_{SE} = U_{SE_{max}} \frac{[Ca^{2+}]_o^4}{K_{1/2}^4 + [Ca^{2+}]_o^4} \quad (1)$$

84 where  $U_{SE}$  is the absolute release probability and  $U_{SE_{max}}$  and  $K_{1/2}$  are free parameters.  $K_{1/2}$   
85 values were taken from Rozov et al. (2001), 2.79 (mM) for steep and 1.09 (mM) for shallow  
86 calcium dependence and were shown to generalize well for other characterized pathways of the  
87 neocortex (see Supplementary Figure S11 in Markram et al. (2015)). In the absence of hip-  
88 pocampus specific data, we followed the approach of Markram et al. (2015) and assumed a steep  
89 dependence in PC to PC and PC to distal dendrite targeting inhibitory (O-LM) cells, and a  
90 shallow dependence between PC to proximal targeting cells (PV+BC (basket cell), CCK+BC,  
91 AAC). For experimentally uncharacterized pathways an intermediate calcium dependence was  
92 used, as the average of the steep and shallow ones. Temperature correction of kinetic parameters  
93 such as rise and decay time constants were realized by multiplying them with Q10 scaling factors:

$$\tau_{sim} = \tau_{exp} \times Q10^{(T_{sim} - T_{exp})/10} \quad (2)$$

94 where  $\tau$  is the time constant, Q10 is an empirically determined, receptor-specific parameter,  
95  $T_{sim} = 34^\circ\text{C}$  is the temperature used in the simulations, while  $T_{exp}$  is the temperature of the  
96 experiment. Holding potentials were corrected by the theoretical LJP (Neher, 1992). These  
97 potentials arise from the differences in solutions in the pipette and bath and are in 2-12 mV  
98 range for the standard solutions. Theoretical LJPs were calculated from the reported pipette  
99 and bath solutions with the Clampex 11 software.

### 100 **2.4 Short-term plasticity model fitting**

101 Short-term plasticity (STP) of synapse dynamics was fit by the Tsodyks-Markram (TM) model  
102 (Tsodyks and Markram, 1997). The model assumes that all synaptic connections have a finite  
103 amount of resources. Each presynaptic action potential utilizes a certain fraction of available  
104 resource ( $R$ ) with a release probability ( $U$ ), which then recovers. Over the years, the model  
105 has been refined and enriched to capture for example short-term facilitation and multi-vesicular  
106 release (MVR) (Markram et al., 1998; Loebel et al., 2009). The differential equations are as  
107 follows (see Supplementary Methods for comparison of different versions of the TM model):

$$\frac{dR(t)}{dt} = \frac{1 - R(t)}{D} - U(t)R(t)\delta(t - t_{spike}) \quad (3)$$

108

$$\frac{dU(t)}{dt} = \frac{U_{SE} - U(t)}{F} - U_{SE}(1 - U(t))\delta(t - t_{spike}) \quad (4)$$

109 where  $D$ , and  $F$  and are depression and facilitation recovery time constants respectively,  $U_{SE}$  is  
 110 the absolute release probability also known as the release probability in the absence of facilitation.  
 111  $\delta(t)$  is the Dirac delta function and  $t_{spike}$  indicates the timing of a presynaptic spike. Each action  
 112 potential in a train elicits an  $A_{SE}U(t_{spike})R(t_{spike})$  amplitude PSC, where  $A_{SE}$  is the absolute  
 113 synaptic efficacy.  $R = 1$  and  $U = U_{SE}$  are assumed before the first spike.  $U_{SE}$ ,  $D$ ,  $F$  and  $A_{SE}$  free  
 114 parameters of the model were fit to experimentally recorded PSCs in Kohus et al. (2016) using  
 115 a multiobjective genetic algorithm with BluePyOpt (Van Geit et al., 2016). Different frequency  
 116 stimulations (10, 20 and 40 Hz) were fit together for better generalization. To correctly compare  
 117 the coefficient of variation (CV, std/mean) of first PSC amplitudes, measurement noise was  
 118 added to the simulated traces (Barros-Zulaica et al., 2019). To this end, noise parameters of  
 119 *in vitro* traces were fitted and averaged for every different connection types and then stochastic  
 120 noise generated with these extracted parameters was added to the corresponding *in silico* traces.  
 121 Noise was described as an Ornstein-Uhlenbeck (OU) process. The OU process is a stationary  
 122 Gauss-Markov process, which describes the velocity of the movement of a Brownian particle and  
 123 is used in physics to describe noise relaxation (Bibbona et al., 2008). Mathematically it can be  
 124 described with the following iterative equation:

$$X(i) = X(i-1) - \frac{X(i-1)}{\tau}dt + \sigma\sqrt{\frac{2dt}{\tau}}\mathcal{N}(0,1) \quad (5)$$

125 where  $dt$  is the time step of the signal,  $\tau$  is the time constant fit to the exponential decay of the  
 126 signal's autocorrelation function,  $\sigma$  is the standard deviation of the signal and  $\mathcal{N}(0,1)$  is a draw  
 127 from the normal distribution.

## 128 2.5 In silico synapse model

129 The synapse model used in the simulations is based on the classical quantal model (Del Castillo  
 130 and Katz, 1954), in which a synaptic connection is assumed to be composed of  $N$  independent  
 131 release sites, each of which has a probability of release,  $p$  (function of  $U_{SE}$ ,  $D$ ,  $F$ ), and contributes  
 132 a quanta  $q$  (function of the conductance  $g(t)$ ) to the postsynaptic response (Ramaswamy et al.,  
 133 2012, 2015; Markram et al., 2015; Chindemi, 2018). Conductances were modeled with double  
 134 exponential kinetics:

$$g(t) = \hat{g}(d(t) - r(t)) \quad (6)$$

$$\frac{dd(t)}{dt} = -\frac{d(t)}{\tau_d} + A\frac{N_r}{N_{RRP}}\delta(t - t_{spike}) \quad (7)$$

$$\frac{dr(t)}{dt} = -\frac{r(t)}{\tau_d} + A\frac{N_r}{N_{RRP}}\delta(t - t_{spike}) \quad (8)$$

$$A = -e^{-t_p/\tau_r} + e^{-t_p/\tau_d} \quad (9)$$

$$t_p = \frac{\tau_d\tau_r}{(\tau_d - \tau_r)\log(\tau_d/\tau_r)} \quad (10)$$

139 where  $\hat{g}$  (nS) is the peak conductance,  $d$  is the decaying component with time constant  $\tau_d$  (ms)  
 140 and  $r$  is the rising component with time constant  $\tau_r$  (ms). Rise time constants are set to 0.2 ms for  
 141 all pathways following Markram et al. (2015). Synapses were normalized (with  $A$  normalization  
 142 constant) such as they reach peak conductance at time to peak  $t_p$  (ms).  $N_r$  is the number  
 143 of released vesicles. Vesicle release dynamics was governed by a hybrid stochastic STP model  
 144 (Fuhrmann et al., 2002). The model releases a single vesicle with probability  $U(t)$  (see TM model  
 145 above) which then recovers. Vesicle recovery is an explicit process, meaning that compared to the  
 146 canonical TM model, only fully recovered vesicles can be released. To this end, synaptic vesicles  
 147 were implemented as 2-state (effective and recovering) Markov processes, in which staying in the

148 recovered state at time  $t$  was described as a survival process, with time constant  $D$  (Chindemi,  
149 2018):

$$P_{surv}(t) = e^{-(t-t_{spike})/D} \quad (11)$$

150 The above-described model converges to the canonical TM model in the limit (number of trials  
151  $\rightarrow \infty$ ). MVR was implemented as  $N$  independent vesicles being released with the same prob-  
152 ability  $U(t)$ .  $N_{RRP}$  is the size of the readily releasable pool of vesicles and normalizing with it  
153 can be seen as scaling down the quantal size  $q$  of the quantal model in case of MVR, to keep  
154 the same mean PSP amplitudes, while changing only the variance (Barros-Zulaica et al., 2019).  
155  $N_{RRP}$  was tuned to match the CVs of first PSC amplitudes from Kohus et al. (2016). Due to  
156 the lack of available raw data with STP protocol (and electron microscopy confirmation of the  
157 number of functional release sites) for most connections, the assumption of MVR (Conti and  
158 Lisman, 2003; Christie and Jahr, 2006) with  $N_{RRP} = 2$  vesicles at each excitatory to excitatory  
159 terminal was used in this study, while all remaining non-tuned pathways were assumed to release  
160 single vesicles. See eg. Biro et al. (2005) and Gulyás et al. (1993) suggesting uni-vesicular release  
161 (UVR) for certain PC to interneuron connections. AMPAr and GABAr synaptic currents are  
162 then computed as:

$$I(t) = g(t)(V_m(t) - E_{rev}) \quad (12)$$

163 where  $V_m$  (mV) is the membrane potential and  $E_{rev}$  (mV) is the reversal potential of the given  
164 synapse. NMDAr currents depend also on  $Mg^{2+}$  block:

$$I_{NMDA}(t) = g(t)mg(V)(V_m(t) - E_{rev}) \quad (13)$$

165 where  $mg(V)$  is the LJP corrected Jahr-Stevens nonlinearity (Jahr and Stevens, 1990):

$$mg(V) = \frac{1}{1 + e^{-c_1 V_m C / c_2}} \quad (14)$$

166 where  $C$  is the extracellular magnesium concentration and  $c_1 = 0.062$  (1/mV) and  $c_2 = 2.62$   
167 (mM) are constants. NMDAr rise and decay time constants are Q10 corrected (Hestrin et al.,  
168 1990; Korinek et al., 2010) values from Andrasfalvy and Magee (2001):  $\tau_r = 3.9$  ms,  $\tau_d = 148.5$   
169 ms. Peak NMDAr conductance  $\hat{g}_{NMDA}$  (nS) is calculated from the AMPAr one by multiplying it  
170 with NMDA/AMPA peak conductance ratio. NMDA/AMPA peak conductance ratio = 1.22 was  
171 taken from Groc et al. (2002); Myme et al. (2003). Synaptic currents are individually delayed  
172 based on axonal path length and conduction velocity of  $300 \mu\text{m}/\text{ms}$  (Stuart et al., 1997) and an  
173 additional 0.1 ms delay of neurotransmitter release (Ramaswamy et al., 2012).

## 174 2.6 Peak conductance tuning via in silico paired recordings

175 Paired recordings were replicated in silico as follows: Firstly, pairs were selected from the circuit  
176 based on distance criteria used by experimentalist (100  $\mu\text{m}$  cube for cells in the same layer and 200  
177  $\mu\text{m}$  cube for cell pairs from different layers). Secondly, postsynaptic cells were current-clamped to  
178 match the LJP-corrected holding potential specified in the experiments. It is important to note,  
179 that in the case of pyramidal cells sodium channels were blocked (*in silico* TTX application)  
180 when clamping above -60 mV to avoid spontaneous firing of the cell models (see Figure 5 in  
181 Migliore et al. (2018)). Thirdly, a spike from the presynaptic cell was triggered, which stimulated  
182 all the synapses of the connection and resulted in a somatic PSP of the postsynaptic neuron.  
183 This exercise was run for 50 pairs with 35 repetitions for each. Lastly, mean PSP amplitude  
184 was compared to the experimentally reported one and peak conductance value was adjusted  
185 respectively using the formula:

$$\hat{g} = \hat{g} \frac{PSP_{exp}(1 - PSP_{model})/df}{PSP_{model}(1 - PSP_{exp})/df} \quad (15)$$

186 where  $PSP_{exp}$  (mV) and  $PSP_{model}$  (mV) are the experimental and modeled PSPs amplitudes  
187 respectively and  $df = |E_{rev} - V_{hold}|$  (mV) is the driving force.  $E_{rev} = 0$  mV was used for  
188 excitatory connections, while  $E_{rev} = -80$  mV for the inhibitory ones. All simulations were run  
189 using the NEURON simulator as a core engine (Hines and Carnevale, 1997) with the Blue Brain  
190 Project's collection of .hoc and NMODL (Hines and Carnevale, 2000) templates for parallel  
191 execution on supercomputers (Hines et al., 2008a,b).

## 192 2.7 Statistical analysis

193 R values for validating matching experimental and model values are Pearson correlations. Data  
194 are presented as mean $\pm$ std to yield comparable values to the experimental ones.

## 195 3 Results

196 The unifying workflow used to integrate synaptic data about the hippocampal CA1 is presented  
197 in Figure 1 and results from our literature review, parameter fitting and modeling will be detailed  
198 step-by-step in the following sections.

### 199 3.1 Literature curation

200 Firstly, we undertook an extensive literature review of paired recording experiments, and com-  
201 piled data on the various parameters (see Supplementary Table S1 for voltage clamp, and Supple-  
202 mentary Table S2 for current clamp recordings from rat hippocampal CA1). The data collected  
203 in this manner is sparse and inhomogeneous, due to the diversity of experimental conditions  
204 used by different labs and were corrected for various aspects.  $[Ca^{2+}]_o$  is known to affect release  
205 probability and additional Hill scaling had to be considered when parametrizing STP profiles  
206 (see Methods). Rise and decay time constants of synaptic currents are influenced by tempera-  
207 ture differences but can be corrected with Q10 factors (see Methods). For electrophysiological  
208 recordings patch pipettes are becoming the standard practice over sharp electrodes nowadays,  
209 however, care should be taken when using absolute potentials reported from publications using  
210 whole-cell patch-clamp recordings (see Methods).

### 211 3.2 Validation of synapse anatomy and dendritic attenuation

212 Before we ran any simulations with synapses using the extracted parameters, we verified that  
213 the anatomy of synapses (Figure 2) such as the number of synapses per connection and targeting  
214 profile, as well as basic electrophysical properties of the cell models match experimental data.  
215 Cell pairs used in the simulations were pulled out from a data-driven reconstruction of the rat  
216 CA1 region, built with the pipeline presented in Markram et al. (2015). Number of synapses per  
217 connection for experimentally characterized pathways (Ali, 2011; Biro et al., 2005; Buhl et al.,  
218 1994a,b; Deuchars and Thomson, 1996; Földy et al., 2010; Maccaferri et al., 2000; Sik et al.,  
219 1995; Vida et al., 1998) ( $r = 0.98$ , Figure 2 b and Supplementary Table S3) along with targeting  
220 profile (Figure 2 a) was verified for this work. PSP attenuation in the active dendrites of PCs  
221 (Migliore et al., 2018) is also in line with the experimentally reported curves (Magee and Cook,  
222 2000) (Supplementary Figure S1).

### 223 3.3 Short-term plasticity of synapses

224 Transmission properties of hippocampal CA1 neurons were demonstrated to express a wide range  
225 of STP profiles in response to presynaptic trains of action potentials at different frequencies (Ali

226 et al., 1998, 1999; Ali and Thomson, 1998; Élteš et al., 2017; Kohus et al., 2016; Losonczy et al.,  
227 2002; Pouille and Scanziani, 2004). However, to our best knowledge, only Losonczy et al. (2002)  
228 and Kohus et al. (2016) reported TM model parameters for CA1 pathways and used additional  
229 recovery spike after the spike train, which is crucial to distinguish pseudo-linear profiles from  
230 purely facilitating or depressing ones. Published STP parameters from Losonczy et al. (2002)  
231 were used for PC to basket cell pathways, after refitting a subset of their data and confirming  
232 the similarity between our resulting  $U_{SE}$ ,  $D$ ,  $F$  values. Kohus et al. (2016) also took the effort  
233 to make their raw traces publicly available, thus despite all the differences from our standard  
234 approach (current-clamp recordings from rat at  $[Ca^{2+}]_o = 2$  mM) we used their traces to fit the  
235 parameters (see Methods) of the TM model (Tsodyks and Markram, 1997; Markram et al., 1998).  
236 We rigorously validated that our event-based amplitude fitting is equivalent to the equations  
237 previously presented in the literature (Markram et al., 1998; Maass and Markram, 2002) (see  
238 Supplementary Methods). Fitted parameters matched well the ones fitted in the original article  
239 (Kohus et al., 2016), despite the slight differences in the TM model used, and the CVs of the  
240 first PSC amplitudes, which were not used during the fitting (see Methods) were also close to  
241 experimental ones ( $r = 0.8$ , Figure 3 b, Supplementary Table S4). (CCK+ dendrite targeting  
242 interneurons were used as Schaffer collateral-associated cells.) For PV+BC to PC and PV+BC  
243 we had to introduce MVR (see Methods) (with  $N_{RRP} = 6$  vesicles) to match the CVs of the  
244 measured PSCs (Figure 3 b). On the other hand, *in silico* PV+BC to AA PSCs had lower CVs  
245 with UVR than the *in vitro* ones, which could not be corrected. (MVR can reduce the variance,  
246 but not increase). Biró et al. (2006) have shown in an elegant study, that while CCK+BC to PC  
247 connections in CA3 are characterized by MVR (with  $N_{RRP} = 5-7$  vesicles) under experimentally  
248 imposed high release probability conditions (high extracellular Ca/Mg ratio), at physiologically  
249 relevant  $[Ca^{2+}]_o$  UVR is more prevalent. In our simulations, the CV of the *in silico* CCK+BC  
250 to PC PSCs matched well the *in vitro* ones, recorded under physiological conditions using UVR,  
251 in good agreement with the Biró et al. (2006) study. For the remaining pathways  $U_{SE}$ ,  $D$ ,  $F$   
252 values from the analogous pathways of the somatosensory cortex (Markram et al., 2015) were  
253 used since parameters of the comparable connections matched well (perisomatic inhibitory to PC,  
254 inhibitory to inhibitory) and that is the most comprehensive dataset available to date. Based  
255 on the literature and our model-fitting we identified several rules to characterize and group STP  
256 profiles. The characterization of all pathways result as follows (Table 1, Figure 4): PC to O-LM  
257 cells (Ali and Thomson, 1998; Biro et al., 2005; Losonczy et al., 2002; Pouille and Scanziani, 2004)  
258 and other interneurons in stratum oriens (Élteš et al., 2017) E1 (excitatory facilitating). PC to  
259 PC (Deuchars and Thomson, 1996), PC to all SOM- interneurons (Ali et al., 1998; Losonczy  
260 et al., 2002; Pouille and Scanziani, 2004) E2 (excitatory depressing). CCK+ interneurons to  
261 CCK+ interneurons (Ali, 2007, 2011; Kohus et al., 2016) I1 (inhibitory facilitating), PV+ and  
262 SOM+ interneurons to PC (Ali et al., 1998, 1999; Bartos et al., 2002; Buhl et al., 1995; Daw et al.,  
263 2009; Kohus et al., 2016; Maccaferri et al., 2000; Pawelzik et al., 2002) as well as interneurons  
264 to interneurons (except the CCK+ ones) (Bartos et al., 2002; Daw et al., 2009; Elfant et al.,  
265 2008; Karayannis et al., 2010; Kohus et al., 2016; Price et al., 2005) I2 (inhibitory depressing).  
266 CCK+ and NOS+ (only Ivy cells, since we lack NGF morphologies) to PC (Fuentelba et al.,  
267 2008; Kohus et al., 2016; Price et al., 2008) I3 (inhibitory pseudo linear). It is important to note  
268 here that these profiles are valid in juvenile animals at  $[Ca^{2+}]_o = 2$  mM, but in some cases,  
269 release probability scales drastically with  $[Ca^{2+}]_o$  and the STP profiles can change as well. For  
270 example, at an *in vivo* like calcium level (1.1-1.3 mM) the PC to PC pathway can show an  
271 E3 (excitatory pseudo-linear) characteristic with amplitudes having a lower mean and higher  
272 trial-by-trial variability and more failures compared to the *in vitro* (2 mM) depressing E2 profile  
273 (Supplementary Figure 2 b). As a function of  $[Ca^{2+}]_o$   $U_{SE}$  values (absolute release probability  
274 parameter of the TM model) are scaled by Hill isotherm (see Methods) parametrized with cortical

275 data of PSP amplitude changes (Supplementary Figure S11 in [Markram et al. \(2015\)](#)). Here we  
276 have shown that applying this scaling function on the absolute release probabilities indeed results  
277 in the same scaling profile of PSP amplitudes in the case of PC to PC connection (Supplementary  
278 Figure 2 a).

### 279 **3.4 Tuning of peak conductances to match PSP amplitudes**

280 Peak conductances of single synapses cannot be measured routinely with today's experimental  
281 techniques, thus are always somehow tuned to match a desired behavior in modeling studies.  
282 While it is appealing to calculate peak conductances from voltage-clamp recordings simply by  
283 dividing peak PSC amplitudes by the driving forces and plug them into a synapse model, it should  
284 not be done because of the space clamp artifacts ([Bar-Yehuda and Korngreen, 2008](#); [Spruston  
285 et al., 1993](#); [Williams and Mitchell, 2008](#)). Namely, if one voltage clamps the soma of a neuron,  
286 that will not necessarily mean that the dendritic compartments where most of the synapses arrive  
287 will have the same holding voltage (which cannot be compensated experimentally) and this can  
288 bias the driving force estimate. Furthermore, in the case of thin dendrites and strong synapses,  
289 the relation between the PSC amplitude and the peak conductance is rather sublinear ([Gulyás  
290 et al., 2016](#)). Using the same reasoning and access to connections measured in both voltage  
291 clamp and current clamp modes from the somatosensory cortex we have recently shown that the  
292 space clamp corrected *in silico* peak conductances are at least twice as big as their calculated  
293 counterparts ([Markram et al., 2015](#)). In the case of rat hippocampal CA1, we did not have the  
294 luxury of having both PSCs and PSPs from the same pair (See Supplementary Tables S1 and S2),  
295 thus just used all PSPs to tune the *in silico* peak conductances to match the *in vitro* PSPs ([Ali  
296 et al., 1998](#); [Ali and Thomson, 1998](#); [Cobb et al., 1997](#); [Deuchars and Thomson, 1996](#); [Fuentealba  
297 et al., 2008](#); [Pawelzik et al., 1999, 2002](#)) (Figure 3 d, Table 1). In short, all other synapse  
298 parameters (anatomy, rise, and decay time constants, STP parameters,  $N_{RRP}$ , NMDA/AMPA  
299 peak conductance ratio, reversal potential) were rigorously validated, a pair was selected from the  
300 digitally reconstructed circuit, the postsynaptic neuron was current clamped to the given holding  
301 voltage, a spike was delivered from the presynaptic neuron, which caused a PSP, measured in  
302 the soma. After repeating this for multiple pairs ( $n = 50$ ) with many trials for each ( $n = 35$ ) we  
303 scaled the peak conductance to match the reference mean PSP amplitude (see Methods). Next,  
304 we repeated the same protocol on a different set of randomly selected 50 pairs with the tuned peak  
305 conductance distributions as a validation of the reconstruction process itself ( $r = 0.99$ , Figure 3 d,  
306 Supplementary Table S5). As an external validation of the resulting peak conductances, we set to  
307 compare them to published single-channel conductance and receptor number estimates. We only  
308 found sufficient data in the case of excitatory connections to PCs. CA1 PCs receive most of their  
309 excitatory inputs from CA3 PCs by the Schaffer collaterals ([Megías et al., 2001](#); [Takács et al.,  
310 2012](#)), whereas in the present article we only considered internal connections (eg. excitatory  
311 connections between CA1s) and no long-range projections. Thus, single-channel conductance  
312 and receptor number estimates from the Schaffer collateral synapses were assumed to generalize  
313 for the internal PC to PC connections (Table 2). Using non-stationary fluctuation analysis on  
314 EPSCs recorded in outside-out dendritic membrane patches, [Spruston et al. \(1995\)](#) estimated  
315 10.2 pS AMPA and 43.5 pS NMDA single-channel conductances. Using these numbers, our  
316 tuned  $0.6 \pm 0.1$  nS AMPA peak conductance (Table 1) is the net result of  $\sim 59$  AMPA and  $\sim 18$   
317 NMDA receptors (with 1.33 NMDA/AMPA peak conductance ratio, see Methods). In their *in  
318 vitro* study, [Spruston et al. \(1995\)](#) estimated 58 – 70 AMPA and 5 – 30 NMDA receptors ([Jonas  
319 et al., 1993](#)), which align well with our *in silico* predictions. MPA receptor numbers were also  
320 estimated with a quantitative immunogold localization technique ([Nusser et al., 1998](#)), as well  
321 as by non-stationary fluctuation analysis on single-spine level following two-photon glutamate  
322 uncaging ([Matsuzaki et al., 2001](#)) and these numbers also parallel with our predictions. Taken



323 together, these data serve as an independent validation of the tuned peak conductance of the  
324 most important, PC to PC pathway. Predicted average GABA conductance is  $1.8 \pm 0.6$  nS, which  
325 corresponds to  $\sim 90$  GABA receptors, which is also in good agreement with general estimates  
326 for the central nervous system (Mody and Pearce, 2004).

### 327 3.5 Parameter generalization

328 After integrating all the parameters (Table 1), obtaining values from somatosensory cortex to  
329 fill knowledge gaps when necessary (Table 1), and simulating paired recordings *in silico* we  
330 could extend predictions derived through this framework to other pathways (Figure 3 c, e).  
331 Synapse anatomy of the experimentally uncharacterized pathways was assumed to be correct  
332 and missing kinetic parameters were filled in with average values from the known ones, grouped  
333 by neurochemical markers, targeting and STP profiles and peak conductances (Table 1). This  
334 exercise resulted in 9 classes, covering all connection types in the CA1 region (Table 1, Figure  
335 4). All the assumptions used in this study leading to the set of presented model parameters  
336 are listed in Table 2. Among other values, we predicted the first PSP amplitudes of all possible  
337 connections (Figure 3 e), given our cell models (Migliore et al., 2018) and connectivity. An  
338 exemplar rare case of more than one published value for a given synaptic property in the literature  
339 is the notion of “strong” connection between PCs and CA1 interneurons (Gulyás et al., 1993),  
340 which could not be used directly for tuning because the postsynaptic target was not clear,  
341 but was confirmed after generalization and *in silico* experiments with all possible postsynaptic  
342 interneurons (Figure 3 e). It is important to note, that due to the highly detailed nature of our  
343 digital, data-driven reconstruction process not only mean pathway values (Figure 3 c, e) but also  
344 detailed distributions can be predicted with the framework (Figure 3 f).

### 345 3.6 Synaptic strength

346 It is general practice among modelers using simplified models to represent synapses as single  
347 contacts between neurons and parameterize them with a single “weight”. It is important to note  
348 that in the detailed models presented here to concept of “weight” is a result of several features not  
349 just the peak conductance. This concept depends on the number and location of synapses (Figure  
350 2), dendritic attenuation (Supplementary Figure S1), NMDA/AMPA conductance ratio and the  
351 interplay between release probability, number of vesicles and peak conductance. As an example,  
352 connections made by interneurons targeting perisomatic regions of PCs are mediated by multiple  
353 synapses with almost no attenuation, however have large peak conductances to compensate for  
354 the relatively low release probability (Table 1, Figure 4 h, i). They are characterized by low  $U_{SE}$   
355 values (in our stochastic model the release probability almost always equals  $U_{SE}$  for depressing  
356 connections) and thus a high trial-to-trial variance. A notable exception from this high trial-to-  
357 trial variance is the PV+BC to PC pathway (Figure 3 a, f), which is more reliable (Figure 3 f.6)  
358 thanks to the MVR with 6 independent synaptic vesicles per a single synapse.

## 359 4 Discussion

360 Recent advances in high-performance computing have enabled biologically detailed, data-driven  
361 reconstructions and large-scale simulations of brain regions (Bezaire and Soltesz, 2013; Bezaire  
362 et al., 2016; Markram et al., 2015; Wheeler et al., 2015). In the present study, we have demon-  
363 strated that a data-driven workflow grounded in biological first-principles, which was used to  
364 digitally reconstruct a biologically detailed model of rat neocortical tissue, can be extended to  
365 model other brain regions such as the hippocampal CA1, to reconcile disparate cellular and

366 synaptic data, and to predictively extrapolate the sparse set of parameters to synaptic connections that have not yet been characterized experimentally. It is known that  $[Ca^{2+}]_o$  regulates the neurotransmitter release probability, and therefore, the amplitudes of PSPs. In this study we adapted the existing data-driven digital reconstruction workflow to reconcile differences in synaptic dynamics that were characterized at different levels of extracellular calcium. Therefore, we scaled the neurotransmitter release probabilities for all pathways that were characterized at 1.6-2 mM  $[Ca^{2+}]_o$  (Kohus et al., 2016; Losonczy et al., 2002; Markram et al., 2015) before tuning peak conductances to match PSP amplitudes that were measured at 2.5 mM  $[Ca^{2+}]_o$ , which is more representative of baseline values for slice experiments (Ali et al., 1998; Ali and Thomson, 1998; Deuchars and Thomson, 1996; Fuentealba et al., 2008; Pawelzik et al., 1999, 2002).

367  
368  
369  
370  
371  
372  
373  
374  
375  
376 In the continuing spirit of unifying hippocampal synaptic electrophysiology from published literature a recent complementary study leveraged text-mining techniques to extract the properties of synaptic connections in hippocampal CA1, including PSP amplitudes and peak conductances (Moradi and Ascoli, 2019). However, our approach to data integration from literature demonstrates that synaptic properties reported in the literature such as peak conductances should not be interpreted on face value but require further corrections to account for inadequate space-clamp errors, which could severely underestimate their value by two-three fold (Markram et al., 2015).

377  
378  
379  
380  
381  
382  
383 The results we report, to the best of our knowledge, constitute a comprehensive resource for not only for the anatomy but also the kinetic and short-term dynamic physiological properties of the rat hippocampal CA1 region. Consolidation of the state of the literature not only facilitates building detailed models, but also highlights knowledge gaps and could help in prioritizing the identification of missing data on CA1 connections, such as PC to interneurons, and between interneurons, which are key building blocks of feedback inhibition. Indeed, the parameter set presented here should be considered a first draft, which will be systematically refined as and when new experimental data become available. By detailing all the integration steps in this study, we had two main objectives. First, we aimed to demonstrate that published parameters should not be taken at face value without rigorously checking their consistency within any modeling framework, and the necessity of being abreast of the state-of-the-art experimental techniques. Second, we attempted to emphasize the fact that a growing diversity of experimental standards combined with published literature that provides access to only processed data sets but not raw experimental traces could lead to an inconsistent picture of a fundamental mechanism such as synaptic transmission. The bottom-up modeling framework presented as a resource in this article could enable ways to integrate disparate data and provide a platform in catalyzing community-driven consensus on the synaptic organization of the hippocampal formation.

## 400 Acknowledgements

401 We would like to thank Giuseppe Chindemi, Natali Barros-Zulaica, Rodrigo Perin and Zoltán Nusser for fruitful discussions as well as Werner Van Geit, Michael Gevaert, Arseniy Povolotsky, Cyrille Favreau and Marwan Abdellah for technical assistance. An initial version of this manuscript was submitted to bioRxiv.

## 405 Author contribution

406 S.R., E.M. and A.R. conceptualized and supervised the study. S.K., M.M., A.M. and H.M. contributed to the supervision of the study. A.R. built the CA1 circuit with inputs from all authors. S.S. validated PSP attenuation. A.E. curated literature, performed simulations, analysis and created the figures with inputs from S.R. A.E. and S.R. wrote the manuscript with inputs from all authors.

410 **Funding**

411 The ETH Domain for the Blue Brain Project (BBP); The Human Brain Project through the European  
412 Union Seventh Framework Program (FP7/2007-2013) under grant agreement no. 604102 (HBP) and  
413 from the European Union H2020 FET program through grant agreement no. 720270 (HBP SGA1); The  
414 Cajal Blue Brain Project (MINECO); The BlueBrain V. HPE SGI 8600 system is financed by ETH  
415 Board Funding to the Blue Brain Project as a National Research Infrastructure and hosted at the Swiss  
416 National Supercomputing Center (CSCS).

417 **Conflict of interest**

418 The authors declare that the research was conducted in the absence of any commercial or financial  
419 relationships that could be construed as a potential conflict of interest.

420 **Tables**

**Table 1: Parameters and generalization to 9 classes.** Table with model synapse parameters either extracted from the literature ( $\tau_d$  (ms)), fitted ( $U_{SE}$ ,  $D$  (ms),  $F$  (ms)), tuned ( $\hat{g}$ (nS)) or taken from the somatosensory cortex (marked with \*) (Markram et al., 2015). Average class parameters are marked in bold and are used predictively for the remaining pathways belonging to the same class. Abbreviations are as in **Figure 2 b**

Pre	Post	$\hat{g}$	$\tau_d$	$U_{SE}$	$D$	$F$	$N_{RRP}$
<b>PC to PC (E2)</b>							
PC	PC	0.6±0.1	3±0.2	0.5±0.02*	671±17*	17±5*	2
<b>PC to SOM+ (E1)</b>							
<b>PC</b>	<b>SOM+</b>	<b>0.85±0.1</b>	<b>1.7±0.14*</b>	<b>0.09±0.12*</b>	<b>138±211*</b>	<b>670±830*</b>	1
<b>PC to SOM- (E2)</b>							
PC	PVBC	3±0.3	4.12±0.5	0.23±0.09	410±190	10±11	1
PC	CCKBC	3.8±0.3	<b>4.12±0.5</b>	0.23±0.09	410±190	10±11	1
PC	BS	1.4±0.1	<b>4.12±0.5</b>	<b>0.23±0.09</b>	<b>410±190</b>	<b>10±11</b>	1
PC	Ivy	5±0.5	<b>4.12±0.5</b>	<b>0.23±0.09</b>	<b>410±190</b>	<b>10±11</b>	1
<b>PC</b>	<b>SOM-</b>	<b>3.3±1.3</b>	<b>4.12±0.5</b>	<b>0.23±0.09</b>	<b>410±190</b>	<b>10±11</b>	1
<b>PV+ to PC (I2)</b>							
PVBC	PC	1.75±0.1	5.45±0.5	0.16±0.02	965±185	8.6±4.3	6
AA	PC	2.35±0.2	<b>6.1±0.68</b>	0.1±0.01	1278±760	10±6.7	1
BS	PC	2.4±0.3	6.81±0.42	<b>0.13±0.03</b>	<b>1122±156</b>	<b>9.3±0.7</b>	1
<b>PV+</b>	<b>PC</b>	<b>2.15±0.3</b>	<b>6.1±0.68</b>	<b>0.13±0.03</b>	<b>1122±156</b>	<b>9.3±0.7</b>	1
<b>CCK+ to PC (I3)</b>							
CCKBC	PC	1.7±0.3	6.5±0.3	0.16±0.04	153±120	12±3.5	1
SCA	PC	2.25±0.3	8.3±0.44	0.15±0.03	185±32	14±5.8	1
<b>CCK+</b>	<b>PC</b>	<b>1.9±0.27</b>	<b>7.5±0.9</b>	<b>0.16±0.01</b>	<b>168±15</b>	<b>13±0.5</b>	1
<b>SOM+ to PC (I2)</b>							
Tri	PC	1.3±0.3	7.75±0.9	<b>0.3±0.08*</b>	<b>1250±520*</b>	<b>2±4*</b>	1
<b>SOM+</b>	<b>PC</b>	<b>1.3±0.3</b>	<b>8.3±2.2*</b>	<b>0.3±0.08*</b>	<b>1250±520*</b>	<b>2±4*</b>	1
<b>NOS+ to PC (I3)</b>							
Ivy	PC	0.55±0.05	8.3±2.2*	0.32±0.14*	144±80*	62±31*	1
<b>I to I (I2)</b>							
PVBC	PVBC	2.2±0.3	2.67±0.13	0.26±0.05	930±360	1.6±0.6	6
PVBC	AA	<b>2.2±0.3</b>	<b>2.67±0.13</b>	0.24±0.15	1730±530	3.5±1.5	1
<b>I</b>	<b>I</b>	<b>2.2±0.3</b>	<b>2.67±0.13</b>	<b>0.26±0.05</b>	<b>930±360</b>	<b>1.6±0.6</b>	1
<b>CCK+ to CCK+ (I1)</b>							
CCKBC	CCKBC	<b>2.2±0.3</b>	4.5±0.55	0.11±0.03	115±110	1542±700	1
SCA	SCA	<b>2.2±0.3</b>	<b>4.5±0.55</b>	<b>0.11±0.03</b>	<b>115±110</b>	<b>1542±700</b>	1

**Table 2: List of assumptions.** All the assumptions that were made to arrive at model parameters from a sparse set of raw data and published values.

- 
- 1 When using data from [Kohus et al. \(2016\)](#) we assumed that CCK+DTI neurons are SCA cells in SR. Furthermore, we assumed that synaptic currents measured in mouse CA3 are representative for similar pathways in rat CA1.
  - 2 We assume that after all the listed correction in this paper, all parameters coming from different sources can be used together to parameterize the synapse models.
  - 3 In lack of data, we assumed that NMDA/AMPA peak current ratio for excitatory to excitatory connections can be used for excitatory to inhibitory connections as well.
  - 4 Also in the lack of representative data and our lack of neurogliaform cells we assumed that all inhibitory synapses are mediated purely by  $GABA_A$  receptors.
  - 5 For parametrizing reversal potentials we assumed that the general values of 0 mV for excitatory and -80 mV for inhibitory synapses can be used for all pathways.
  - 6 For calculating release probabilities at different extracellular calcium concentrations we assumed that Hill functions parameterized with cortical data generalize well for hippocampal connections.
  - 7 For modeling synaptic currents, we assumed that all CA1 synapses can be described with double exponential conductances, with vesicle release kinetics governed by the TM model.
  - 8 The synapse model presented here, does not account for any type of long-term changes.
  - 9 The biggest assumptions are inherited from the network model: In this work, we assumed that the published electrical models of single cells ([Migliore et al., 2018](#)) capture the behavior of different neurons in rat CA1. (The fact that we can not clamp PC models to potentials above -60mV without blocking sodium channels seems to violate this assumption.) We also assumed that the cell composition and cell density within the layers are homogeneous and the constrained connectivity reflects the connectivity of rat CA1.
  - 10 An inherited assumption from [Markram et al. \(2015\)](#) is that the rise time constant of all synaptic currents is 0.2 ms.
  - 11 Kinetic parameters for a given pathway are drawn from a distribution, but since (almost) all experimental data used to derive these parameters are representative for a given connection and not for individual synapses per se, we use the same parameters for all synapses mediating a single connection.
  - 12 When generalizing our parameters for similar, experimentally uncharacterized pathways we group CA1 interneurons based on only one chemical marker. However, cells express many of these and the markers overlap (see [hippocampome.org](http://hippocampome.org) ([Wheeler et al., 2015](#))). By PV+ cells we mean: SP\_PVBCs, SP\_BS cells and SP\_AA cells. By CCK+ cells we mean: SP\_CCKBCs, SR\_SCA cells and SLM\_PPA cells. The only interneurons in our NOS+ class are SP\_Ivy cells. (Neurogliaform cells would belong here as well.) We assume all neurons in SO: SO\_OLM cells, SO\_BS cells, SO\_Tri cells and SO\_BP cells to be SOM+.
  - 13 A usually unspoken, implicit assumption on communication between neurons is used here as well, namely, we model only glutamatergic and GABAergic synapses between presynaptic axons and postsynaptic somas and dendrites. Thus, we leave out co-transmission and neuromodulators acting on different receptors, retrograde messengers, any kind of gap-junctions and any axonal receptors.
-

## 421 Figure captions

422 **Figure 1. *In silico* data integration pipeline.** **1:** More than a hundred publications were used to  
423 compile data on various parameters of connected neurons in rat CA1. **2:** Parameters were integrated into  
424 a common framework and experimental paradigm, including temperature,  $[Ca^{2+}]_o$  and LJP corrections.  
425 TM models of STP were fit to publicly available raw traces. **3:** *In silico* paired recordings were run to  
426 correctly estimate the unitary peak conductance of connections with experimentally characterized PSP  
427 amplitudes. **4:** Parameters were averaged within classes and used predictively to describe experimentally  
428 uncharacterized pathways.

429  
430 **Figure 2. *In silico* synapse anatomy.** **a:** A representative *in silico* O-LM (purple) to PC (blue)  
431 pair, with synapses visualized in red. 3D morphologies were reconstructed with the NeuroLucida software  
432 (Migliore et al., 2018) by the members of Alex Thomson's lab at UCL. **a.1:** Branch order distribution  
433 ( $n=5000$  connections) of the presynaptic (O-LM) axons. **a.2:** Branch order distribution of the postsy-  
434 naptic (PC) tuft dendrites. **a.3:** Distribution of the number of synapses per connection of the *in silico*  
435 O-LM to PC pathway. *In vitro* experimental data is indicated in red. **a.4:** Distance dependent connection  
436 probability of the *in silico* O-LM to PC pathway. **b:** Validation of the number of synapses per connection  
437 against experimental data. (E: excitatory, I: inhibitory, eg.: I-E: inhibitory to excitatory pathways.) **c:**  
438 Predicted mean number of synapses per connections (within 200  $\mu m$  intersomatic distance) for all path-  
439 ways in the CA1 network model. Layer abbreviations: SR: stratum radiatum, SP: stratum pyramidale,  
440 SO: stratum oriens. M-type (morphological type) abbreviations: AA: axo-axonic cell, BP: back-projecting  
441 cell, BS: bistratified cell, CCKBC: CCK+ basket cell, Ivy: ivy cell, OLM: oriens-lacunosum moleculare  
442 cell, PC: pyramidal cell, PVBC: PV+ basket cell, PPA: performant path-associated cell, SCA: Schaffer  
443 collateral-associated cell, Tri: trilaminar cell. **d:** Predicted mean connection probability (within 200  $\mu m$   
444 intersomatic distance) for all pathways in the CA1 network model. M-type abbreviations are as in **c**.

445  
446 **Figure 3. *In silico* synapse physiology.** **a:** *In silico* paired recording experiment with the STP  
447 protocol used in Kohus et al. (2016). Presynaptic (PV+BC) voltage trace is shown on top. *In silico*  
448 PV+BC (green) to PC (blue) pair, with synapses visualized in red in the middle. 3D morphologies were  
449 reconstructed with the NeuroLucida software (Migliore et al., 2018) by the members of Alex Thomson's  
450 lab at UCL. Postsynaptic (PC) experimental traces recorded *in vitro* (in gray) and their mean in red,  
451 as well as model traces recorded *in silico* (in gray) and their mean in blue, are presented at the bottom  
452 panel. Insets show the variance of the first IPSCs. **b:** Validation of the CV of the first PSC amplitudes  
453 against experimental data. (E: excitatory, I: inhibitory, eg.: I-E: inhibitory to excitatory pathways.)  
454 **c:** Predicted CVs of first PSC amplitudes for all pathways in the CA1 network model after synapse  
455 parameter generalization. 20 pairs with 35 repetitions for every possible connection. Postsynaptic cells  
456 were held at -65 mV in *in silico* voltage-clamp mode. M-type abbreviations are as in **Figure 2 b**. **d:**  
457 Validation of the PSP amplitudes against experimental data. (E: excitatory, I: inhibitory, eg.: I-E: in-  
458 hibitory to excitatory pathways.) **e:** Predicted PSP amplitudes for all pathways in the CA1 network  
459 model after synapse parameter generalization. 20 pairs with 35 repetitions for every possible connection.  
460 Postsynaptic cells were held at -65 mV in *in silico* current-clamp mode. M-type abbreviations are as in  
461 **Figure 2 b**. **f:** Properties of postsynaptic (PC) IPSPs. **f.1:** Distribution of *in silico* PSP amplitudes.  
462 *In vitro* experimental data is indicated in red. **f.2:** Distribution of *in silico* PSP 10-90% rise times. **f.3:**  
463 Distribution of *in silico* PSP decay time constants. **f.4:** Distribution of *in silico* PSP latencies. **f.5:**  
464 Distribution of the CVs of the first *in silico* PSP amplitudes. **f.6:** Distribution of *in silico* failure rates.

465  
466 **Figure 4. Summary of synapse diversity in the CA1 network model.** Panels represent exemplar  
467 *in silico* pairs from the 9 generalized pathways (2 for PC to SOM- interneurons). Presynaptic voltage  
468 traces are shown on the top of the panels, while 35 repetitions (in gray) and their mean postsynaptic  
469 PSPs are presented on the bottom of the panels for each pathway. Postsynaptic cells were held at -65 mV  
470 in *in silico* current-clamp mode. **a:** PC to PC (E2). **b:** PC to O-LM cell (E1). **c:** PC to bistratified cell  
471 (E2). **d:** PC to CCK+BC (E2). **e:** O-LM cell to PC (I2). **f:** CCK+BC to CCK+ BC (I1). **g:** Ivy cell  
472 to PC (I3). **h:** CCK+BC to PC (I3). **i:** PV+BC to PC (I2). **j:** PV+BC to PV+BC (I2). Connectivity  
473 in the schematic CA1 microcircuit in the middle is simplified for visualization purpose (for example most  
474 of the interneuron to interneuron connections are missing). Simplified synapses of the pathways shown  
475 in the panels around are indicated with gray circles. M-type abbreviations are as in **Figure 2 b**.

## 476 References

- 477 Ali, A. B. (2007). Presynaptic Inhibition of GABAA Receptor-Mediated Unitary IPSPs by Cannabi-  
478 noid Receptors at Synapses Between CCK-Positive Interneurons in Rat Hippocampus. *Journal of*  
479 *Neurophysiology*, 98(2):861–869.
- 480 Ali, A. B. (2011). CB1 modulation of temporally distinct synaptic facilitation among local circuit in-  
481 terneurons mediated by N-type calcium channels in CA1. *Journal of Physiology*, 105:1051–1062.
- 482 Ali, A. B., Bannister, A. P., and Thomson, A. M. (1999). IPSPs elicited in CA1 pyramidal cells by putative  
483 basket cells in slices of adult rat hippocampus. *European Journal of Neuroscience*, 11(5):1741–1753.
- 484 Ali, A. B., Deuchars, J., Pawelzik, H., and Thomson, A. M. (1998). CA1 pyramidal to basket and  
485 bistratified cell EPSPs: Dual intracellular recordings in rat hippocampal slices. *Journal of Physiology*,  
486 507(1):201–217.
- 487 Ali, A. B. and Thomson, A. M. (1998). Facilitating pyramid to horizontal oriens-alveus interneurone  
488 inputs: Dual intracellular recordings in slices of rat hippocampus. *Journal of Physiology*, 507(1):185–  
489 199.
- 490 Andrasfalvy, B. K. and Magee, J. C. (2001). Distance-dependent increase in AMPA receptor number in  
491 the dendrites of adult hippocampal CA1 pyramidal neurons. *The Journal of Neuroscience*, 21(23):9151–  
492 9159.
- 493 Bar-Yehuda, D. and Korngreen, A. (2008). Space-Clamp Problems When Voltage Clamping Neurons  
494 Expressing Voltage-Gated Conductances. *Journal of Neurophysiology*, 99(3):1127–1136.
- 495 Barros-Zulaica, N., Rahmon, J., Chindemi, G., Perin, R., Markram, H., Ramaswamy, S., and Muller, E.  
496 (2019). Estimating the Readily-Releasable Vesicle Pool Size at Synaptic Connections in a Neocortical  
497 Microcircuit. *bioRxiv*.
- 498 Bartos, M., Vida, I., Frotscher, M., Meyer, A., Monyer, H., Geiger, J. R. P., and Jonas, P. (2002). Fast  
499 synaptic inhibition promotes synchronized gamma oscillations in hippocampal interneuron networks.  
500 *PNAS*, 99(20):13222–13227.
- 501 Bezaire, M. J., Raikov, I., Burk, K., Vyas, D., and Soltesz, I. (2016). Interneuronal mechanisms of  
502 hippocampal theta oscillations in a full-scale model of the rodent CA1 circuit. *eLife*, 5(e18566):1–106.
- 503 Bezaire, M. J. and Soltesz, I. (2013). Quantitative assessment of CA1 local circuits: Knowledge base for  
504 interneuron-pyramidal cell connectivity. *Hippocampus*, 23(9):751–785.
- 505 Bibbona, E., Panfilo, G., and Tavella, P. (2008). The Ornstein–Uhlenbeck process as a model of a low  
506 pass filtered white noise. *Meteorologia*, 45(6):S117.
- 507 Biro, A. A., Holderith, N. B., and Nusser, Z. (2005). Quantal Size Is Independent of the Release Prob-  
508 ability at Hippocampal Excitatory Synapses. *Journal of Neuroscience*, 25(1):223–232.
- 509 Biró, A. A., Holderith, N. B., and Nusser, Z. (2006). Release probability-dependent scaling of the  
510 postsynaptic responses at single hippocampal GABAergic synapses. *The Journal of neuroscience*,  
511 26(48):12487–96.
- 512 Bliss, T. V. and Collingridge, G. L. (2013). Expression of NMDA receptor-dependent LTP in the hip-  
513 pocampus: bridging the divide. *Molecular Brain*, 6(5).
- 514 Buhl, E. H., Cobb, S. R., Halasy, K., and Somogyi, P. (1995). Properties of unitary IPSPs evoked  
515 by anatomically identified basket cells in the rat hippocampus. *European Journal of Neuroscience*,  
516 7(9):1989–2004.
- 517 Buhl, E. H., Halasy, K., and Somogyi, P. (1994a). Diverse sources of hippocampal unitary inhibitory  
518 postsynaptic potentials and the number of synaptic release sites. *Nature*, 368:823–828.

- 519 Buhl, E. H., Han, Z.-S., Lörinczi, Z., Stezhka, V. V., Karnup, S. V., and Somogyi, P. (1994b). Physiological  
520 Properties of Anatomically Identified AxoAxonic in the Rat Hippocampus. *Journal of Neurophysiology*,  
521 71(4):1289–1307.
- 522 Buzsáki, G. (1989). Two-stage model of memory trace formation: A role for "noisy" brain states. *Neu-*  
523 *roscience*, 31(3):551–570.
- 524 Chindemi, G. (2018). *Towards a unified understanding of synaptic plasticity: parsimonious modeling and*  
525 *simulation of the glutamatergic synapse life-cycle*. PhD thesis, EPFL.
- 526 Christie, J. M. and Jahr, C. E. (2006). Multivesicular Release at Schaffer Collateral-CA1 Hippocampal  
527 Synapses. *Journal of Neuroscience*, 26(1):210–216.
- 528 Cobb, S. R., Halasy, K., Vida, I., Nyíri, G., Tamás, G., Buhl, E. H., and Somogyi, P. (1997). Synaptic  
529 effects of identified interneurons innervating both interneurons and pyramidal cells in the rat hip-  
530 pocampus. *Neuroscience*, 79(3):629–648.
- 531 Conti, R. and Lisman, J. (2003). The high variance of AMPA receptor- and NMDA receptor-mediated  
532 responses at single hippocampal synapses: Evidence for multiquantal release. *PNAS*, 100(8):4885–4890.
- 533 Daw, M. I., Tricoire, L., Erdelyi, F., Szabo, G., and McBain, C. J. (2009). Asynchronous Transmitter  
534 Release from Cholecystokinin-Containing Inhibitory Interneurons Is Widespread and Target-Cell  
535 Independent. *Journal of Neuroscience*, 29(36):11112–11122.
- 536 Del Castillo, J. and Katz, B. (1954). Quantal components of the end-plate potential. *The Journal of*  
537 *Physiology*, 124(3):560–573.
- 538 Deuchars, J. and Thomson, A. M. (1996). CA1 pyramid-pyramid connections in rat hippocampus in  
539 vitro: Dual intracellular recordings with biocytin filling. *Neuroscience*, 74(4):1009–1018.
- 540 Elfant, D., Pal, B. Z., Emptage, N., and Capogna, M. (2008). Specific inhibitory synapses shift the balance  
541 from feedforward to feedback inhibition of hippocampal CA1 pyramidal cells. *European Journal of*  
542 *Neuroscience*, 27(1):104–113.
- 543 Éltés, T., Kirizis, T., Nusser, Z., and Holderith, N. (2017). Target Cell Type-Dependent Differences  
544 in Ca<sup>2+</sup> Channel Function Underlie Distinct Release Probabilities at Hippocampal Glutamatergic  
545 Terminals. *The Journal of Neuroscience*, 37(7):1910–1924.
- 546 Földy, C., Lee, S.-h., Morgan, R. J., and Soltesz, I. (2010). Regulation of fast-spiking basket cell synapses  
547 by the chloride channel ClC-2. *Nature Neuroscience*, 13(9):1047–1049.
- 548 Fuentealba, P., Begum, R., Capogna, M., Jinno, S., Márton, L. F., Csicsvari, J., Thomson, A., Somogyi,  
549 P., and Klausberger, T. (2008). Ivy Cells: A Population of Nitric-Oxide-Producing, Slow-Spiking  
550 GABAergic Neurons and Their Involvement in Hippocampal Network Activity. *Neuron*, 57(6):917–  
551 929.
- 552 Fuhrmann, G., Segev, I., Markram, H., and Tsodyks, M. (2002). Coding of Temporal Information by  
553 Activity-Dependent Synapses. *Journal of Neurophysiology*, 87(1):140–148.
- 554 Groc, L., Gustafsson, B., and Hanse, E. (2002). Spontaneous unitary synaptic activity in CA1 pyramidal  
555 neurons during early postnatal development: constant contribution of AMPA and NMDA receptors.  
556 *The Journal of Neuroscience*, 22(13):5552–5562.
- 557 Gulyás, A. I., Freund, T. F., and Káli, S. (2016). The Effects of Realistic Synaptic Distribution and 3D  
558 Geometry on Signal Integration and Extracellular Field Generation of Hippocampal Pyramidal Cells  
559 and Inhibitory Neurons. *Frontiers in Neural Circuits*, 10(88).
- 560 Gulyás, a. I., Miles, R., Sík, A., Tóth, K., Tamamaki, N., and Freund, T. F. (1993). Hippocampal  
561 pyramidal cells excite inhibitory neurons through a single release site. *Nature*, 366:683–687.



- 562 Hestrin, S., Sah, P., and Nicoll, R. A. (1990). Mechanisms Generating the Time Course of Dual Component  
563 Excitatory Synaptic Currents Recorded in Hippocampal Slices. *Neuron*, 5:247–253.
- 564 Hill, A. V. (1910). The possible effects of the aggregation of the molecules of haemoglobin on its dissociation  
565 curves. *Journal of Physiology*, 40:4–7.
- 566 Hines, M. L. and Carnevale, N. T. (1997). The NEURON simulation environment. *Neural computation*,  
567 9(6):1179–1209.
- 568 Hines, M. L. and Carnevale, N. T. (2000). Expanding NEURON’s repertoire of mechanisms with NMODL.  
569 *Neural Computation*, 12(5):995–1007.
- 570 Hines, M. L., Eichner, H., and Schürmann, F. (2008a). Neuron splitting in compute-bound parallel  
571 network simulations enables runtime scaling with twice as many processors. *Journal of computational  
572 neuroscience*, 25(1):203–210.
- 573 Hines, M. L., Markram, H., and Schürmann, F. (2008b). Fully implicit parallel simulation of single  
574 neurons. *Journal of computational neuroscience*, 25(3):439–448.
- 575 Jahr, C. E. and Stevens, C. F. (1990). Voltage dependence of NMDA-activated macroscopic conductances  
576 predicted by single-channel kinetics. *The Journal of neuroscience*, 10(9):3178–3182.
- 577 Jonas, P., Major, G., and Sakmann, B. (1993). Quantal components of unitary EPSCs at the mossy fibre  
578 synapse on CA3 pyramidal cells of rat hippocampus. *The Journal of Physiology*, 472:615–663.
- 579 Karayannis, T., Elfant, D., Huerta-Ocampo, I., Teki, S., Scott, R. S., Rusakov, D. A., Jones, M. V.,  
580 and Capogna, M. (2010). Slow GABA transient and receptor desensitization shape synaptic responses  
581 evoked by hippocampal neurogliaform cells. *The Journal of neuroscience*, 30(29):9898–909.
- 582 Kohus, Z., Káli, S., Schlingloff, D., Papp, O., Rovira-Esteban, L., Freund, T. F., Hájos, N., and Gulyás,  
583 A. I. (2016). Properties and dynamics of inhibitory synaptic communication within the CA3 microcircuits  
584 of pyramidal cells and interneurons expressing parvalbumin or cholecystokinin. *The Journal of  
585 physiology*, 594(13):3745–74.
- 586 Korinek, M., Sedlacek, M., Cais, O., Dittert, I., and Vyklicky, L. (2010). Temperature dependence  
587 of N-methyl-d-aspartate receptor channels and N-methyl-d-aspartate receptor excitatory postsynaptic  
588 currents. *Neuroscience*, 165(3):736–748.
- 589 Loebel, A., Silberberg, G., Helbig, D., Markram, H., Tsodyks, M., and Richardson, M. J. E. (2009).  
590 Multiquantal release underlies the distribution of synaptic efficacies in the neocortex. *Frontiers in  
591 Cellular Neuroscience*, 3(27).
- 592 Losonczy, A., Zhang, L., Shigemoto, R., Somogyi, P., and Nusser, Z. (2002). Cell type dependence and  
593 variability in the short-term plasticity of EPSCs in identified mouse hippocampal interneurons. *The  
594 Journal of physiology*, 542(1):193–210.
- 595 Maass, W. and Markram, H. (2002). Synapses as dynamic memory buffers. *Neural Networks*, 15(2):155–  
596 161.
- 597 Maccaferri, G., Roberts, J. D. B., Szucs, P., Cottingham, C. A., and Somogyi, P. (2000). Cell surface  
598 domain specific postsynaptic currents evoked by identified GABAergic neurones in rat hippocampus  
599 in vitro. *Journal of Physiology*, 524(1):91–116.
- 600 Magee, J. C. and Cook, E. P. (2000). Somatic EPSP amplitude is independent of synapse location in  
601 hippocampal pyramidal neurons. *Nature neuroscience*, 3(9):895–903.
- 602 Markram, H., Wang, Y., and Tsodyks, M. (1998). Differential signaling via the same axon of neocortical  
603 pyramidal neurons. *PNAS*, 95(9):5323–8.
- 604 Markram, M., Muller, E., Ramaswamy, S., Reimann, M. W., et al. (2015). Reconstruction and Simulation  
605 of Neocortical Microcircuitry. *Cell*, 163:456–492.

- 606 Matsuzaki, M., Ellis-Davies, G. C., Nemoto, T., Miyashita, Y., Iino, M., and Kasai, H. (2001). Dendritic  
607 spine geometry is critical for AMPA receptor expression in hippocampal CA1 pyramidal neurons.  
608 *Nature Neuroscience*, 4(11):1086–1092.
- 609 Megías, M., Emri, Z., Freund, T. F., and Gulyás, a. I. (2001). Total number and distribution of inhibitory  
610 and excitatory synapses on hippocampal CA1 pyramidal cells. *Neuroscience*, 102(3):527–540.
- 611 Migliore, R., Lupascu, C. A., Bologna, L. L., Romani, A., Courcol, J.-D., Antonel, S., Van Geit, W.  
612 A. H., Thomson, A. M., Mercer, A., Lange, S., Falck, J., Rössert, C. A., Shi, Y., Hagens, O., Pezzoli,  
613 M., Freund, T. F., Kali, S., Muller, E. B., Schürmann, F., Markram, H., and Migliore, M. (2018).  
614 The physiological variability of channel density in hippocampal CA1 pyramidal cells and interneurons  
615 explored using a unified data-driven modeling workflow. *PLOS Computational Biology*, 14(9):e1006423.
- 616 Mody, I. and Pearce, R. A. (2004). Diversity of inhibitory neurotransmission through GABA A receptors.  
617 *Trends in Neurosciences*, 27(9):569–575.
- 618 Moradi, K. and Ascoli, G. A. (2019). A comprehensive knowledge base of synaptic electrophysiology in  
619 the rodent hippocampal formation. *bioRxiv*, page <http://doi.org/10.1101/632760>.
- 620 Myme, C. I. O., Sugino, K., Turrigiano, G. G., and Nelson, S. B. (2003). The NMDA-to-AMPA Ratio  
621 at Synapses Onto Layer 2/3 Pyramidal Neurons Is Conserved Across Prefrontal and Visual Cortices.  
622 *Journal of Neurophysiology*, 90(2):771–779.
- 623 Neher, E. (1992). Correction for liquid junction potentials in patch clamp experiments. *Methods in*  
624 *Enzymology*, 207:123–131.
- 625 Nusser, Z., Lujan, R., Laube, G., Roberts, J. D. B., Molnar, E., and Somogyi, P. (1998). Cell type and  
626 pathway dependence of synaptic AMPA receptor number and variability in the hippocampus. *Neuron*,  
627 21(3):545–559.
- 628 Pawelzik, H., Bannister, A. P., Deuchars, J., Ilia, M., and Thomson, A. M. (1999). Modulation of  
629 bistratified cell IPSPs and basket cell IPSPs by pentobarbitone sodium, diazepam and Zn<sup>2+</sup>: Dual  
630 recordings in slices of adult rat hippocampus. *European Journal of Neuroscience*, 11(10):3552–3564.
- 631 Pawelzik, H., Hughes, D. I., and Thomson, A. M. (2002). Physiological and morphological diversity of  
632 immunocytochemically defined parvalbumin- and cholecystokinin-positive interneurons in CA1 of the  
633 adult rat hippocampus. *Journal of Comparative Neurology*, 443(4):346–367.
- 634 Pouille, F. and Scanziani, M. (2004). Routing of spike series by dynamic circuits in the hippocampus.  
635 *Nature*, 429(6993):717–723.
- 636 Price, C. J., Cauli, B., Kovács, E. R., Kukik, Á., Lambolez, B., Shigemoto, R., and Capogna, M. (2005).  
637 Neurogliaform Neurons Form a Novel Inhibitory Network in the Hippocampal CA1 Area. *Journal of*  
638 *Neuroscience*, 25(29):6775–6786.
- 639 Price, C. J., Scott, R., Rusakov, D. A., and Capogna, M. (2008). GABAB Receptor Modulation of  
640 Feedforward Inhibition through Hippocampal Neurogliaform Cells. *The Journal of Neuroscience*,  
641 28(27):6974–6982.
- 642 Ramaswamy, S., Courcol, J.-D., Abdellah, M., Adaszewski, S. R., Antille, N., Arsever, S., Atenekeng,  
643 G., Bilgili, A., Brukau, Y., Chalimourda, A., Chindemi, G., Delalondre, F., Dumusc, R., Eilemann, S.,  
644 Gevaert, M. E., Gleeson, P., Graham, J. W., Hernando, J. B., Kanari, L., Katkov, Y., Keller, D., King,  
645 J. G., Ranjan, R., Reimann, M. W., Rössert, C., Shi, Y., Shillcock, J. C., Telefont, M., Van Geit, W.,  
646 Villafranca Diaz, J., Walker, R., Wang, Y., Zaninetta, S. M., DeFelipe, J., Hill, S. L., Muller, J., Segev,  
647 I., Schürmann, F., Muller, E. B., and Markram, H. (2015). The neocortical microcircuit collaboration  
648 portal: a resource for rat somatosensory cortex. *Frontiers in Neural Circuits*, 9(44).
- 649 Ramaswamy, S., Hill, S. L., King, J. G., Schürmann, F., Wang, Y., and Markram, H. (2012). Intrinsic  
650 morphological diversity of thick-tufted layer 5 pyramidal neurons ensures robust and invariant proper-  
651 ties of in silico synaptic connections. *Journal of Physiology*, 590(4):737–752.

- 652 Reimann, M. W., King, J. G., Muller, E. B., Ramaswamy, S., and Markram, H. (2015). An algorithm to  
653 predict the connectome of neural microcircuits. *Frontiers in computational neuroscience*, 9(120).
- 654 Rozov, A., Burnashev, N., Sakmann, B., and Neher, E. (2001). Transmitter release modulation by  
655 intracellular Ca<sup>2+</sup> buffers in facilitating and depressing nerve terminals of pyramidal cells in layer 2/3  
656 of the rat neocortex indicates a target cell-specific difference in presynaptic calcium dynamics. *Journal*  
657 *of Physiology*, 531(3):807–826.
- 658 Sik, A., Penttonen, M., Ylinen, A., and Buzsáki, G. (1995). Hippocampal CA1 Interneurons: An in vivo  
659 Intracellular Labeling Study. *Journal of Neuroscience*, 10(15):6651–6665.
- 660 Spruston, N., Jaffe, D. B., Williams, S. H., and Johnston, D. (1993). Voltage- and space-clamp errors as-  
661 sociated with the measurement of electrotonically remote synaptic events. *Journal of Neurophysiology*,  
662 70(2):781–802.
- 663 Spruston, N., Jonas, P., and Sakmann, B. (1995). Dendritic glutamate receptor channels in rat hip-  
664 pocampal CA3 and CA1 pyramidal neurons. *Journal of Physiology*, 482(2):325–352.
- 665 Stuart, G., Schiller, J., and Sakmann, B. (1997). Action potential initiation and propagation in rat  
666 neocortical pyramidal neurons. *Journal of Physiology*, 505(3):617–632.
- 667 Takács, V. T., Klausberger, T., Somogyi, P., Freund, T. F., and Gulyás, A. I. (2012). Extrinsic and  
668 local glutamatergic inputs of the rat hippocampal CA1 area differentially innervate pyramidal cells  
669 and interneurons. *Hippocampus*, 22(6):1379–1391.
- 670 Tsodyks, M. and Markram, H. (1997). The neural code between neocortical pyramidal neurons depends  
671 on neurotransmitter release probability. *PNAS*, 94:719–723.
- 672 Van Geit, W., Gevaert, M., Chindemi, G., Rössert, C., Courcol, J.-D., Muller, E., Schürmann, F., Segev,  
673 I., and Markram, H. (2016). BluePyOpt: Leveraging open source software and cloud infrastructure to  
674 optimise model parameters in neuroscience. *Frontiers in Neuroinformatics*, 10(17).
- 675 Vida, I., Halasy, K., Szinyei, C., Somogyi, P., and Buhl, E. H. (1998). Unitary IPSPs evoked by in-  
676 terneurons at the stratum radiatum — stratum lacunosum-moleculare border in the CA1. *Journal of*  
677 *Physiology*, 506(3):755–773.
- 678 Wheeler, D. W., White, C. M., Rees, C. L., Komendantov, A. O., Hamilton, D. J., and Ascoli, G. A.  
679 (2015). Hippocampome.org: A knowledge base of neuron types in the rodent hippocampus. *eLife*,  
680 4(e09960).
- 681 Williams, S. R. and Mitchell, S. J. (2008). Direct measurement of somatic voltage clamp errors in central  
682 neurons. *Nature Neuroscience*, 11(7):790–798.

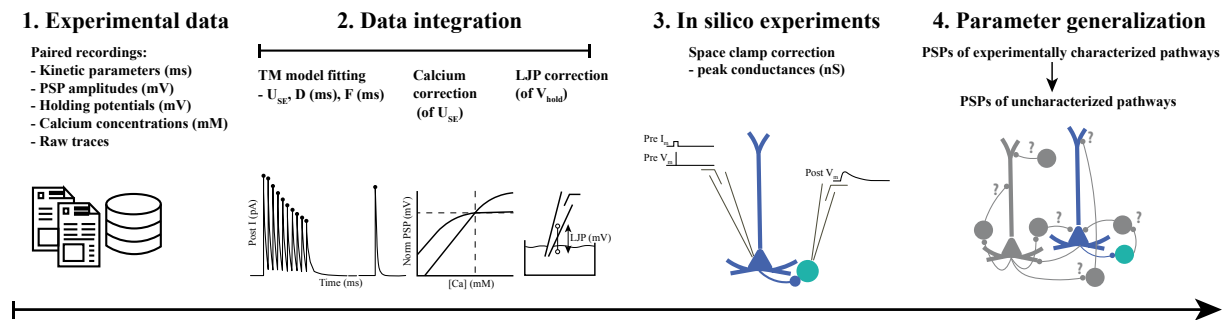


Figure 1 - Ecker et al.

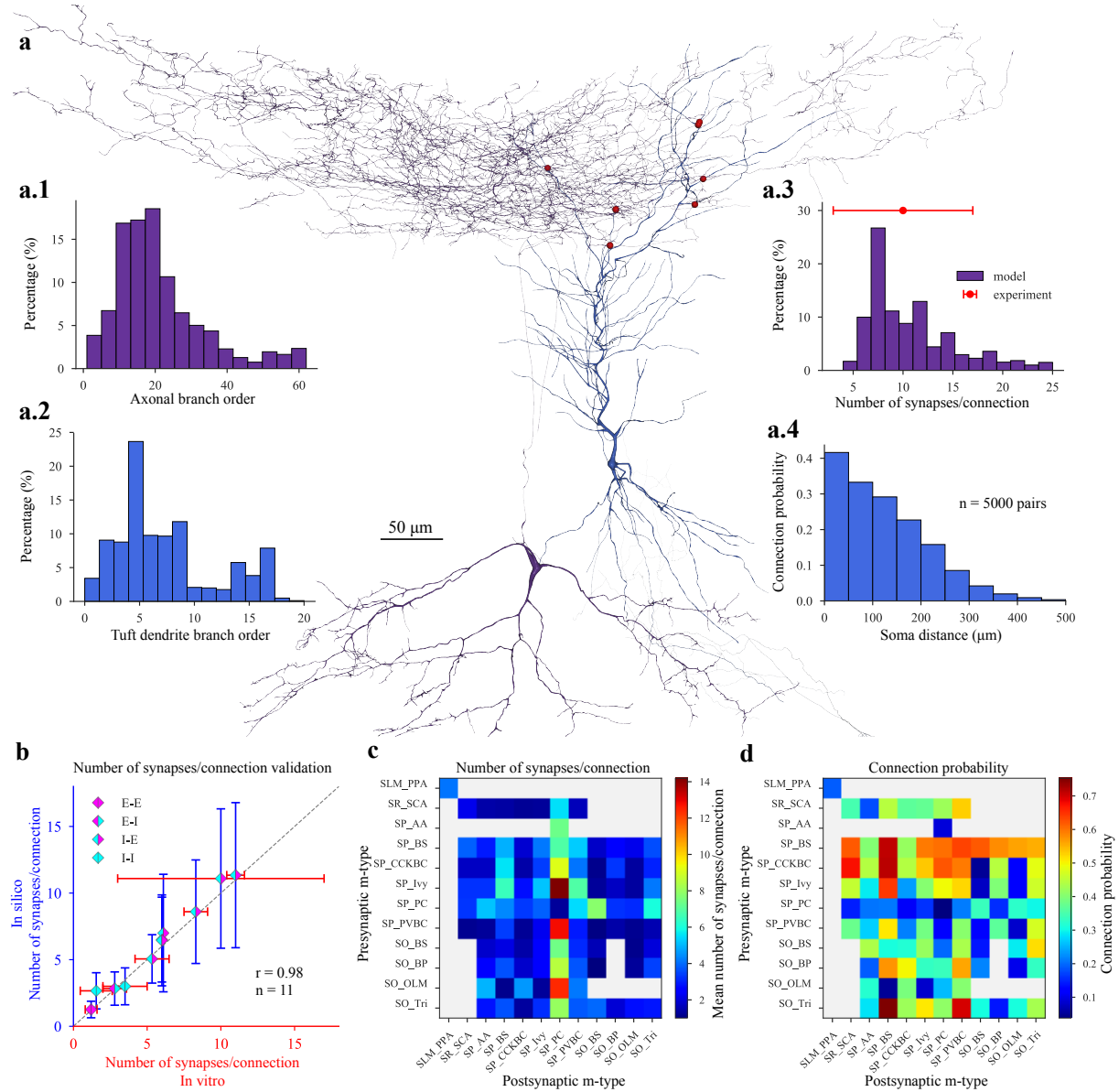


Figure 2 - Ecker et al.

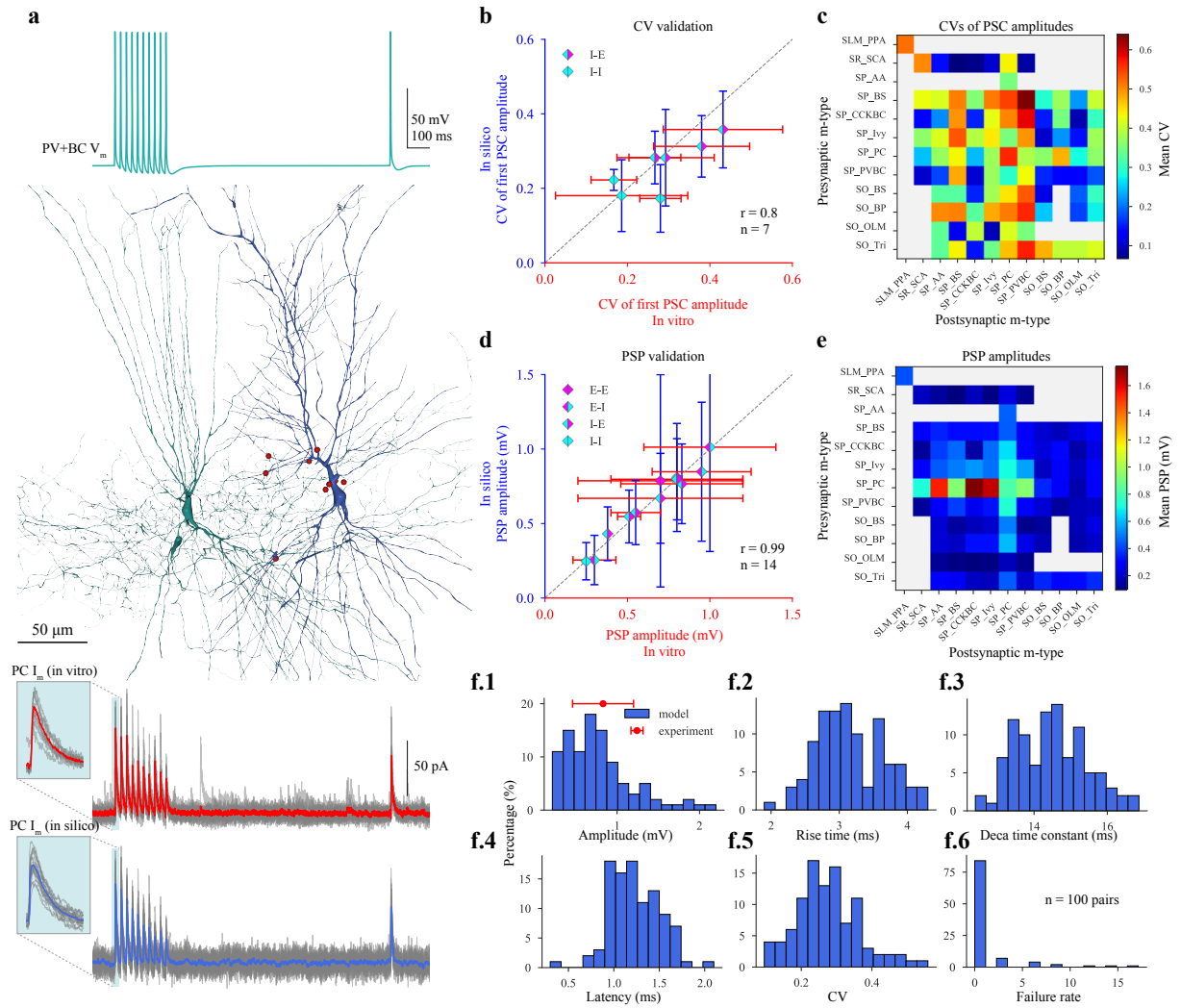


Figure 3 - Ecker et al.

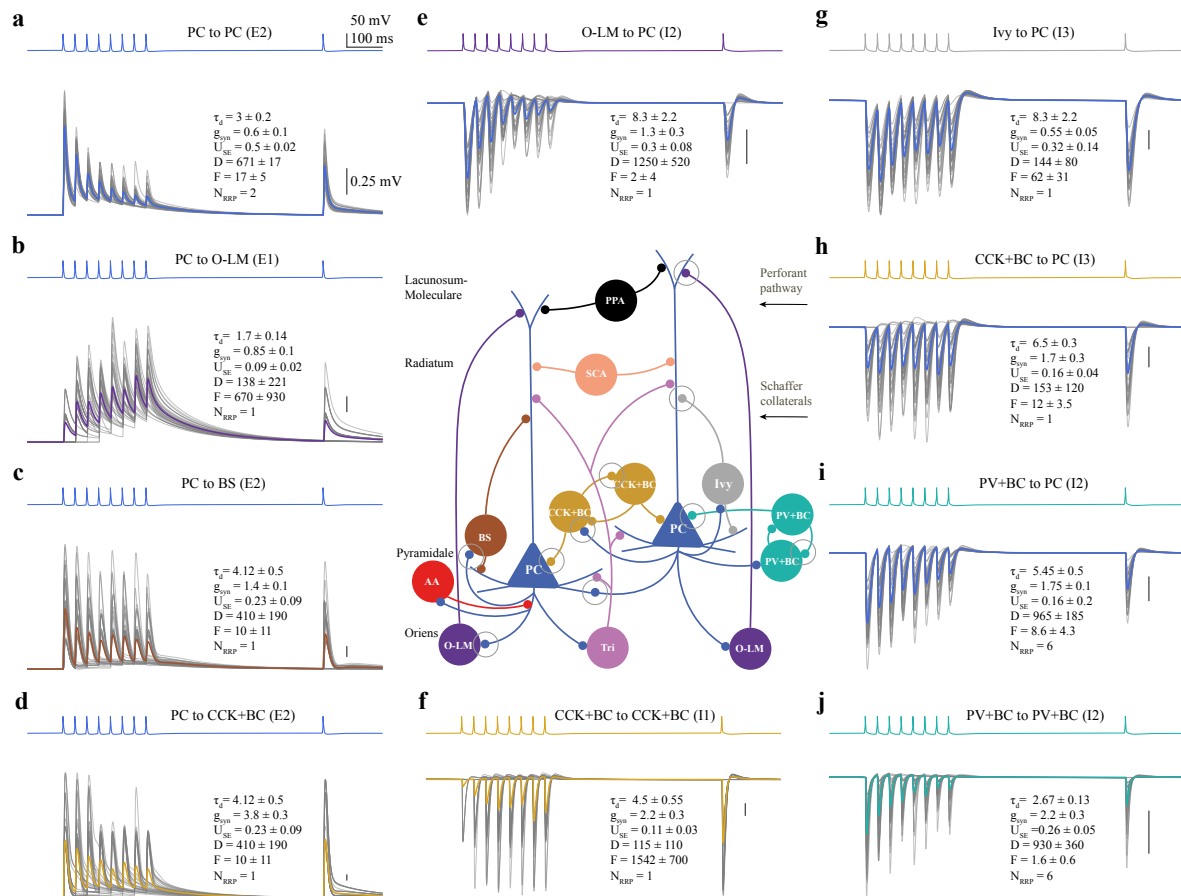


Figure 4 - Ecker et al.

## Supplementary Material: Data-driven integration of hippocampal CA1 synapse physiology in silico

András Ecker, Armando Romani, Sára Sáray, Szabolcs Káli, Michele Migliore, Audrey Mercer, Henry Markram, Eilif Muller, Srikanth Ramaswamy

### Supplementary Methods

The Tsodyks-Markram model of short-term plasticity underwent many changes in the years twenty years. For a recent and consistent review see [Hennig \(2013\)](#). Furthermore, the equations are sometimes shown in the form of differential equations ([Tsodyks and Markram, 1997](#); [Tsodyks et al., 2000](#); [Fuhrmann et al., 2002, 2004](#); [Loebel et al., 2009](#); [Hennig, 2013](#)), while in other papers the iterative solution evaluated at spike arrivals is presented ([Markram et al., 1998](#); [Maass and Markram, 2002](#)). The version used in this article follows the formalism presented in [Hennig \(2013\)](#):

$$\begin{aligned}\frac{dR(t)}{dt} &= \frac{1 - R(t)}{D} - U(t)R(t)\delta(t - t_{spike}) \\ \frac{dU(t)}{dt} &= \frac{U_{SE} - U(t)}{F} + U_{SE}(1 - U(t))\delta(t - t_{spike})\end{aligned}$$

where  $R(t)$  is the fraction of available resources,  $U(t)$  is the release probability,  $D$ , and  $F$  are depression and facilitation time constants respectively.  $U_{SE}$  is the absolute release probability also known as the release probability in the absence of facilitation.  $\delta(t)$  is the Dirac delta function and  $t_{spike}$  indicates the timing of a presynaptic spike. Each action potential in a train elicits an  $A_{SE}U(t_{spike})R(t_{spike})$  amplitude PSC, where  $A_{SE}$  is the absolute synaptic efficacy and is linked to the  $Nq$  part of the quantal model, where  $N$  is the number of release sites and  $q$  is the quantal amplitude.  $R = 1$ , and  $U = U_{SE}$  are assumed before the first spike. In our simulations, we implement [Fuhrmann et al. \(2002\)](#) as the stochastic generalization of the model. The equation of the release probability is slightly different in that article and it reads as follows:

$$\frac{dU(t)}{dt} = -\frac{U(t)}{F} + U_{SE}(1 - U(t))\delta(t - t_{spike})$$

According to this equation  $U(t)$  decays to 0 (the wording of the articles suggest a decay to "the baseline"). To recover the definition of  $U_{SE}$  as the release probability in absence of spikes (or  $U$  as the constant release probability in the first [Tsodyks and Markram \(1997\)](#) paper concentrating only on depressing connections) the  $+U_{SE}(1 - U(t))$  has to be evaluated before the release happens. On the other hand, the  $-U(t)R(t)$  jump in the equation of  $R$  still has to be evaluated after the event in order to be consistent with  $R$  being 1 in the absence of spikes. In this view  $U(t)$  is mostly zero and at spike arrivals, before release happens it jumps to  $U_{SE}$ . From the biophysical point of view, this can be seen as a calcium-based model, where a quick calcium influx leads to release. On the other hand, in the [Hennig \(2013\)](#) version  $U(t)$  decays to its baseline  $U_{SE}$  value and the  $U_{SE}(1 - U(t))$  jump happens after the release. When fitting the deterministic TM model to experimental data as well as simulating the stochastic version we use an event-based solution, meaning that the equations are only evaluated at spike times (as opposed to the ODE form).



For the [Fuhrmann et al. \(2002\)](#) version the iterative update is:

$$\begin{aligned} R_{n+1} &= 1 + (R_n - 1)\exp\left(-\frac{\Delta t}{D}\right) \\ U_{n+1} &= U_n \exp\left(-\frac{\Delta t}{F}\right) \\ U_{n+1} &= U_{n+1} + U_{SE}(1 - U_{n+1}) \\ A_{n+1} &= A_{SE}U_{n+1}R_{n+1} \\ R_{n+1} &= R_{n+1} - U_{n+1}R_{n+1} \end{aligned}$$

where  $\Delta t$  is the the time between the  $(n + 1)$ th and  $n$ th spike and  $A_n$  is the  $n$ th amplitude. On the other hand, the [Hennig \(2013\)](#) version (used to fit models in [Kohus et al. \(2016\)](#)) is:

$$\begin{aligned} R_{n+1} &= 1 + (R_n - 1)\exp\left(-\frac{\Delta t}{D}\right) \\ U_{n+1} &= U_{SE} + (U_n - U_{SE})\exp\left(-\frac{\Delta t}{F}\right) \\ A_{n+1} &= A_{SE}U_{n+1}R_{n+1} \\ R_{n+1} &= R_{n+1} - U_{n+1}R_{n+1} \\ U_{n+1} &= U_{n+1} + U_{SE}(1 - U_{n+1}) \end{aligned}$$

None of these forms are presented in the literature. Both [Markram et al. \(1998\)](#) and [Maass and Markram \(2002\)](#) put the jump terms into the decaying exponential part as follows:

$$\begin{aligned} R_{n+1} &= 1 + (R_n - 1 - U_n R_n)\exp\left(-\frac{\Delta t}{D}\right) \\ U_{n+1} &= U_{SE} + (U_n - U_{SE} + U_{SE}(1 - U_n))\exp\left(-\frac{\Delta t}{F}\right) \\ &= U_{SE} + U_n(1 - U_{SE})\exp\left(-\frac{\Delta t}{F}\right) \\ &= U_n \exp\left(-\frac{\Delta t}{F}\right) + U_{SE}(1 - U_n \exp\left(-\frac{\Delta t}{F}\right)) \\ A_{n+1} &= A_{SE}U_{n+1}R_{n+1} \end{aligned}$$

Using the initialization  $R_1 = 1$ ,  $U_1 = U_{SE}$  and calculating the first two amplitudes with all 3 versions ([Fuhrmann et al. \(2002\)](#), [Hennig \(2013\)](#) and [Maass and Markram \(2002\)](#)) one gets:

$$\begin{aligned} A_1 &= A_{SE}U_{SE} \\ A_2 &= A_{SE}[U_{SE} + (U_{SE} - U_{SE}^2)\exp\left(-\frac{\Delta t}{F}\right)](1 - U_{SE}\exp\left(-\frac{\Delta t}{D}\right)) \end{aligned}$$

With simulations, it is also possible to show that all the other amplitudes in response to a spike train will be the same for all versions. Thus, the 3 event-based models presented above are equivalent even if it would be hard to confirm by algebra. We present the [Hennig \(2013\)](#) formalism in the article since we find it more intuitive that both Dirac deltas are evaluated at the same point (after the PSC amplitude is calculated) and is more in line with the wording of the papers, but emphasize that it is consistent with the other versions and the fits presented in [Markram et al. \(2015\)](#).

## Supplementary Figures

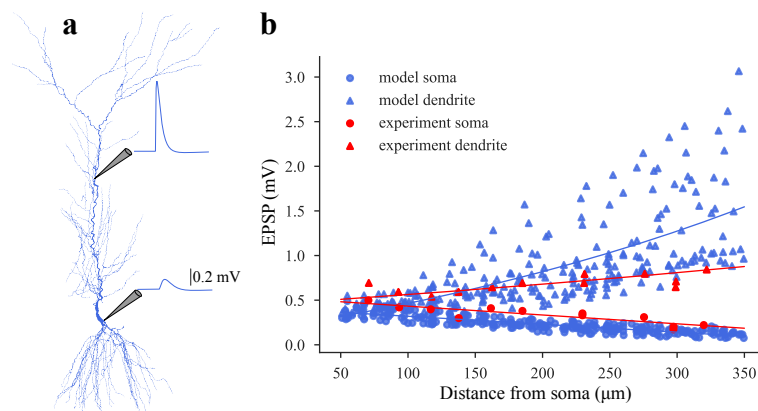


**Figure S1: PSP attenuation.** Validation of PSP attenuation against experimental data from [Magee and Cook \(2000\)](#). **a:** EPSC like currents were injected to the apical dendrites of the different pyramidal cell models from [Migliore et al. \(2018\)](#) and PSPs were measured at the injection site and at the soma. **b:** Summary of all models injected at different sites (in blue) and comparison to experimental data (in red).

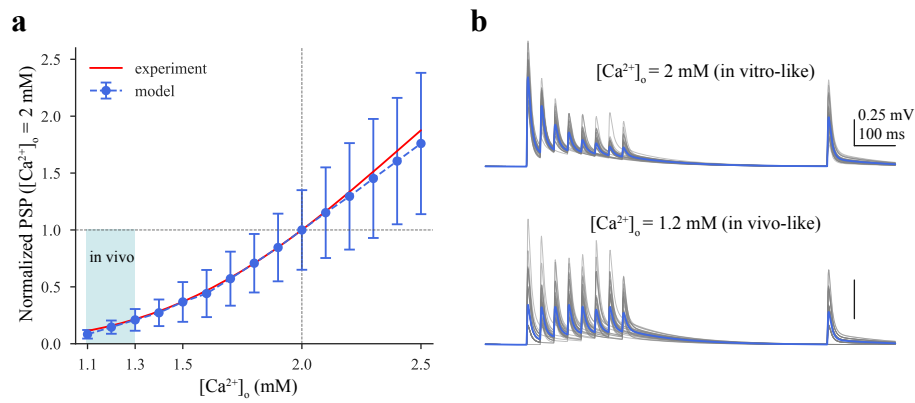


**Figure S2: Calcium sensitivity of synaptic physiology.** **a:** PC to PC PSP amplitudes at different extracellular calcium concentrations (normalized to 2 mM). Red curve indicates the experimentally measured scaling function which was applied to scale the  $U_{SE}$  parameter of the TM model. Shaded light blue area indicates the *in vivo* range 1.1-1.3 mM. **b:** Same *in silico* PC to PC pair at two different extracellular calcium concentrations. *In vitro* like is shown on top, while the *in vivo* one at the bottom. Single trials ( $n=35$ ) are shown in gray and their average in blue. Postsynaptic cells were held at -65 mV in *in silico* current-clamp mode.

## Supplementary Tables

**Table S1:** Summary of paired recording experiments from CA1 in voltage-clamp mode (PSCs in pA). Holding potentials are not corrected for the indicated liquid junction potential. \* in the rise time constant column indicates 20-80% rise time, instead of 10-90%. Abbreviations are as in **Figure 2 b**

Presyn.	Postsyn.	Animal	Elect.	Ampl. (pA)	Rise (ms)	Decay (ms)	Hold. (mV)	[Ca <sup>2+</sup> ] (mM)	Temp. [°C]	LJP (mV)	Reference
AA	PC	rat (P10-17)	patch	308±103	0.8±0.1	11.2±0.9	-70	3	~30	-	<a href="#">Maccaferri et al. (2000)</a>
BS	PC	rat (P10-17)	patch	Fig6) A,B	2±0.2	16.1±1.1	-70	3	~30	-	<a href="#">Maccaferri et al. (2000)</a>
CCKBC	PC	rat (P16-20)	patch	118±13	0.73±0.05	6.8±0.2	-70	2	33	-	<a href="#">Neu et al. (2007)</a>
CCKBC	PC	rat (P16-21)	patch	53.7±17.2	-	-	-70	2	33	-	<a href="#">Földy et al. (2007)</a>
CCKBC	PC	rat (P17-22)	patch	115.4±10.8	0.63±0.04	6.47±0.27	-58.3±0.5	2	33	-	<a href="#">Lee et al. (2010)</a>
NGF	PC	rat (P18-24)	patch	4.9±1	-	50±4.9	-50±2	2.5	33±2	12	<a href="#">Price et al. (2008)</a>
OLM	PC	rat (P10-17)	patch	26±10	6.2±0.6	20.8±1.7	-70	3	~30	-	<a href="#">Maccaferri et al. (2000)</a>
PVBC	PC	rat (P16-21)	patch	43.6±17.9	-	-	-70	2	33	-	<a href="#">Földy et al. (2007)</a>
SCA	PC	rat (P17-22)	patch	60.2±8.1	1.43±0.12	8.3±0.44	-58.1±0.8	2	33	-	<a href="#">Lee et al. (2010)</a>
NGF	NGF	rat (P12-21)	patch	20.97±23.68		42.05±22.03	-50	2.5	33-35	-	<a href="#">Price et al. (2005)</a>
NGF	NGF	rat (P18-22)	patch	85.3±9.6	3.69±0.34*	60.3±4.7	-65	2	33±1	-	<a href="#">Karayannis et al. (2010)</a>
OLM	NGF	rat (P18-20)	patch	19.2	2.2	10.8	-50	2	33±1	-	<a href="#">Elfant et al. (2008)</a>
OLM	PVBC	rat (P18-20)	patch	11.7±1	2.6±1.3	16.5±3.9	-50	2	33±1	-	<a href="#">Elfant et al. (2008)</a>
OLM	SCA	rat (P18-20)	patch	19.5±4.7	1.9±0.4	31.2±4.5	-50	2	33±1	-	<a href="#">Elfant et al. (2008)</a>

**Table S2:** Summary of paired recording experiments from CA1 in current-clamp mode (PSPs in mV). No LJP correction is necessary since all recordings were obtained with sharp electrodes. \* in the half width column indicates decay time constant instead of half width. Abbreviations are as in **Figure 2 b**

Presyn.	Postsyn.	Animal	Elect.	Ampl. (mV)	Rise (ms)	HalfW (ms)	Hold. (mV)	[Ca <sup>2+</sup> ] (mM)	Temp. [°C]	LJP (mV)	Reference
PC	PC	rat (100-180g)	sharp	0.7±0.5	2.7±0.19	16.8±4.1	-67-70	2.5	34-36	∅	Deuchars and Thomson (1996)
AA	PC	rat (90-160g)	sharp	0.51±0.07	5±0.2	45.6±2	-53±1	2.5	34-36	∅	Pawelzik et al. (1999)
BS	PC	rat (90-160g)	sharp	0.86±0.55	8.5±3.6	43.9±13.9	-57.6±4.4	2.5	34-36	∅	Pawelzik et al. (1999)
BS	PC	rat (120-200g)	sharp	0.55±0.15	7.4±1.4	54.6±4.2	-58.5±0.5	2.	34-36	∅	Pawelzik et al. (2002)
BS	PC	rat (140-200g)	sharp	0.8±0.6	8.4±3.2	42.1±17	-53	2.5	33±1	∅	Fuentealba et al. (2008)
CCKBC	PC	rat (120-200g)	sharp	1.17±0.44	5.4±2.5	35.5±19.5	-65-85	2.5	34-36	∅	Ali et al. (1999)
CCKBC	PC	rat (100-200g)	sharp	1.47±1.06	6±2.2	47.6±13.3	-55-60	2.5?	34-36	∅	Thomson et al. (2000)
CCKBC	PC	rat (120-200g)	sharp	0.7±0.5	6.5±1.5	44.2±10.1	-58.6±3.3	2.5	34-36	∅	Pawelzik et al. (2002)
Ivy	PC	rat (140-200g)	sharp	0.8±0.4	2.8±0.2	54.1±13.8	-57	2.5	33±1	∅	Fuentealba et al. (2008)
PV+BC	PC	rat (150g<)	sharp	0.45±0.24	4.6±3.2	32.4±18*	-57.8±4.6	2	34-35	∅	Buhl et al. (1995)
PV+BC	PC	rat (120-200g)	sharp	1.17±0.57	4.5±2	30.4±11.6	-65-85	2.5	34-36	∅	Ali et al. (1999)
PV+BC	PC	rat (90-160g)	sharp	0.81±0.92	6.8±2.7	47.2±16.9	-54.7±3.8	2.5	34-36	∅	Pawelzik et al. (1999)
PVBC	PC	rat (100-200g)	sharp	1.12±0.74	5.1±1.8	39.5±15.2	-55-60	2.5?	34-36	∅	Thomson et al. (2000)
PVBC	PC	rat (120-200g)	sharp	0.83±0.37	5.13±2.06	38.32±12	-58.4±3	2.5	34-36	∅	Pawelzik et al. (2002)
SCA	PC	rat (120-200g)	sharp	0.38	10±2.8	45±2.2	-58.5±0.5	2.5	34-36	∅	Pawelzik et al. (2002)
Tri	PC	rat (120-200g)	sharp	0.8	5.6	48.8	-58.5±0.5	2.5	34-36	∅	Pawelzik et al. (2002)
PC	BS	rat (90-180g)	sharp	3.4±3.1	1.2±0.5	7.6±2.6	-66	2.5	34-35	∅	Ali et al. (1998)
PC	BS	rat (120-200g)	sharp	0.95±0.3	1.2±0.2	10.4±1.6	-66±1	2.5	34-36	∅	Pawelzik et al. (2002)
PC	BS	rat (140-200g)	sharp	1.8±2.3	1.5±0.3	6.4±2.7	-60	2.5	33±1	∅	Fuentealba et al. (2008)
PC	CCKBC	rat (120-200g)	sharp	2±2.1	1±0.4	6.1±1.5	-67±3	2.5	34-36	∅	Pawelzik et al. (2002)
PC	Ivy	rat (140-200g)	sharp	2.9±2.2	1.5±0.3	11.5±1.5	-60	2.5	33±1	∅	Fuentealba et al. (2008)
PC	OLM	rat (90-150g)	sharp	0.93±1.06	1.2±0.5	7.5±0.7	-70±2.3	2.5	34-36	∅	Ali and Thomson (1998)
PC	PVBC	rat (90-180g)	sharp	1.4±1.05	0.88±0.44	5.4±2.2	-66	2.5	34-35	∅	Ali et al. (1998)
PC	PVBC	rat (120-200)	sharp	3.51±2.9	1±0.3	5.74±1.78	-67	2.5	34-36	∅	Pawelzik et al. (2002)
BC	BS	rat (150g)	sharp	0.37	1	5.6	-55	2	34-35	∅	Cobb et al. (1997)
BC	BS	rat (120-180g)	sharp	1±0.4	1.65±0.5	15.6±2.8	-63±4.4	2.5	34-36	∅	Pawelzik et al. (2003)
BC	BC	rat (150g)	sharp	0.25	1.3	27	-59	2	34-35	∅	Cobb et al. (1997)
BC	BC	rat (120-180g)	sharp	1.1±0.47	2.5±0.9	18.7±9.1	-59±4	2.5	34-36	∅	Pawelzik et al. (2003)
BS	BC	rat (120-180g)	sharp	0.7±0.4	2.5±0.8	19.1±9.5	-59.7±2.7	2.5	34-36	∅	Pawelzik et al. (2003)
SCA	SCA	rat (120-200g)	sharp	0.5	5	34.3	-58	2.5	34-36	∅	Pawelzik et al. (2002)
SCA	SCA	rat (P18-23)	patch	0.6±0.41	7.0±1.38	41.1±12.5	-55	2	20-22	-	Ali (2007)

**Table S3:** Validation of number of synapses per connections. See **Figure 2 b**). Abbreviations are as in **Figure 2 b**

Presyn.	Postsyn.	Reference data	Model	Reference
PC	PC	1.2±0.4	1.26±0.6	<a href="#">Deuchars and Thomson (1996)</a>
AA	PC	6.1	7±4.4	<a href="#">Buhl et al. (1994b)</a>
BS	PC	6	6.5±3.2	<a href="#">Buhl et al. (1994a)</a>
CCKBC	PC	8.3±0.8	8.6±3.9	<a href="#">Földy et al. (2010)</a>
OLM	PC	10±7	11±5.2	<a href="#">Maccaferri et al. (2000)</a>
PVBC	PC	11±0.6	11.3±5.4	<a href="#">Földy et al. (2010)</a>
SCA	PC	5.3±1.2	5±1.8	<a href="#">Vida et al. (1998)</a>
PC	OLM	2.8±0.8	2.8±1.2	<a href="#">Biro et al. (2005)</a>
PVBC	PV+	1.54±1.08	2.6±1.3	<a href="#">Sik et al. (1995)</a>
SCA	SCA	3.5±1.5	3±1.4	<a href="#">Ali (2011)</a>

**Table S4:** Validation of the CV of first PSC amplitudes. See **Figure 3 b**). Abbreviations are as in **Figure 2 b**

Presyn.	Postsyn.	Reference data	Model	Reference
AA	PC	$0.29 \pm 0.11$	$0.28 \pm 0.13$	<a href="#">Kohus et al. (2016)</a>
CCKBC	PC	$0.43 \pm 0.14$	$0.36 \pm 0.1$	<a href="#">Kohus et al. (2016)</a>
PVBC	PC	$0.26 \pm 0.06$	$0.28 \pm 0.07$	<a href="#">Kohus et al. (2016)</a>
SCA	PC	$0.38 \pm 0.11$	$0.31 \pm 0.08$	<a href="#">Kohus et al. (2016)</a>
CCKBC	CCKBC	$0.18 \pm 0.16$	$0.18 \pm 0.1$	<a href="#">Kohus et al. (2016)</a>
PVBC	AA	$0.45 \pm 0.11$	$0.17 \pm 0.09$	<a href="#">Kohus et al. (2016)</a>
PVBC	PVBC	$0.17 \pm 0.05$	$0.22 \pm 0.02$	<a href="#">Kohus et al. (2016)</a>

**Table S5:** Validation of PSP amplitudes. See **Figure 3 d**). PC to CCKBC and PC to Ivy are not shown on the figure for visualization purpose. In some cases (indicated with \*) outliers were removed from the reference data (see published reference data in Table S1). Abbreviations are as in **Figure 2 b**

Presyn.	Postsyn.	Reference data (mV)	Model (mV)	Reference
PC	PC	0.7±0.5	0.78±0.71	<a href="#">Deuchars and Thomson (1996)</a>
AA	PC	0.51±0.07	0.55±0.17	<a href="#">Pawelzik et al. (1999)</a>
BS	PC	0.55±0.15	0.57±0.21	<a href="#">Pawelzik et al. (2002)</a>
CCKBC	PC	0.7±0.5	0.67±0.3	<a href="#">Pawelzik et al. (2002)</a>
Ivy	PC	0.8±0.4	0.8±0.27	<a href="#">Fuentealba et al. (2008)</a>
PVBC	PC	0.83±0.37	0.76±0.26	<a href="#">Pawelzik et al. (2002)</a>
SCA	PC	0.38	0.43±0.18	<a href="#">Pawelzik et al. (2002)</a>
Tri	PC	0.8	0.8±0.36	<a href="#">Pawelzik et al. (2002)</a>
PC	BS	0.95±0.3	1±0.54	<a href="#">Pawelzik et al. (2002)</a>
PC	CCKBC	2±2.1	1.9±1.35	<a href="#">Pawelzik et al. (2002)</a>
PC	Ivy	2.9±2.2	2.45±1.5	<a href="#">Fuentealba et al. (2008)</a>
PC	OLM	0.3±0.13*	0.25±0.16	<a href="#">Ali and Thomson (1998)</a>
PC	PVBC	1±0.4*	1±0.7	<a href="#">Ali et al. (1998)</a>
(PV)BC	(PV)BC	0.25	0.25±0.12	<a href="#">Cobb et al. (1997)</a>



## References

- Ali, A. B. (2007). Presynaptic Inhibition of GABAA Receptor-Mediated Unitary IPSPs by Cannabinoid Receptors at Synapses Between CCK-Positive Interneurons in Rat Hippocampus. *Journal of Neurophysiology*, 98(2):861–869.
- Ali, A. B. (2011). CB1 modulation of temporally distinct synaptic facilitation among local circuit interneurons mediated by N-type calcium channels in CA1. *Journal of Physiology*, 105:1051–1062.
- Ali, A. B., Bannister, A. P., and Thomson, A. M. (1999). IPSPs elicited in CA1 pyramidal cells by putative basket cells in slices of adult rat hippocampus. *European Journal of Neuroscience*, 11(5):1741–1753.
- Ali, A. B., Deuchars, J., Pawelzik, H., and Thomson, A. M. (1998). CA1 pyramidal to basket and bistratified cell EPSPs: Dual intracellular recordings in rat hippocampal slices. *Journal of Physiology*, 507(1):201–217.
- Ali, A. B. and Thomson, A. M. (1998). Facilitating pyramid to horizontal oriens-alveus interneurone inputs: Dual intracellular recordings in slices of rat hippocampus. *Journal of Physiology*, 507(1):185–199.
- Biro, A. A., Holderith, N. B., and Nusser, Z. (2005). Quantal Size Is Independent of the Release Probability at Hippocampal Excitatory Synapses. *Journal of Neuroscience*, 25(1):223–232.
- Buhl, E. H., Cobb, S. R., Halasy, K., and Somogyi, P. (1995). Properties of unitary IPSPs evoked by anatomically identified basket cells in the rat hippocampus. *European Journal of Neuroscience*, 7(9):1989–2004.
- Buhl, E. H., Halasy, K., and Somogyi, P. (1994a). Diverse sources of hippocampal unitary inhibitory postsynaptic potentials and the number of synaptic release sites. *Nature*, 368:823–828.
- Buhl, E. H., Han, Z.-S., Lörinczi, Z., Stezhka, V. V., Karnup, S. V., and Somogyi, P. (1994b). Physiological Properties of Anatomically Identified AxoAxonic in the Rat Hippocampus. *Journal of Neurophysiology*, 71(4):1289–1307.
- Cobb, S. R., Halasy, K., Vida, I., Nyíri, G., Tamás, G., Buhl, E. H., and Somogyi, P. (1997). Synaptic effects of identified interneurons innervating both interneurons and pyramidal cells in the rat hippocampus. *Neuroscience*, 79(3):629–648.
- Deuchars, J. and Thomson, A. M. (1996). CA1 pyramid-pyramid connections in rat hippocampus in vitro: Dual intracellular recordings with biocytin filling. *Neuroscience*, 74(4):1009–1018.
- Elfant, D., Pal, B. Z., Emptage, N., and Capogna, M. (2008). Specific inhibitory synapses shift the balance from feedforward to feedback inhibition of hippocampal CA1 pyramidal cells. *European Journal of Neuroscience*, 27(1):104–113.
- Földy, C., Lee, S.-h., Morgan, R. J., and Soltesz, I. (2010). Regulation of fast-spiking basket cell synapses by the chloride channel ClC-2. *Nature Neuroscience*, 13(9):1047–1049.
- Földy, C., Lee, S. Y., Szabadics, J., Neu, A., and Soltesz, I. (2007). Cell type – specific gating of perisomatic inhibition by cholecystokinin. *Nature neuroscience*, 10(9):1128–1130.
- Fuentealba, P., Begum, R., Capogna, M., Jinno, S., Márton, L. F., Csicsvari, J., Thomson, A., Somogyi, P., and Klausberger, T. (2008). Ivy Cells: A Population of Nitric-Oxide-Producing, Slow-Spiking GABAergic Neurons and Their Involvement in Hippocampal Network Activity. *Neuron*, 57(6):917–929.

- Fuhrmann, G., Cowan, A., Segev, I., Tsodyks, M., and Stricker, C. (2004). Multiple mechanisms govern the dynamics of depression at neocortical synapses of young rats. *Journal of Physiology*, 557(2):415–438.
- Fuhrmann, G., Segev, I., Markram, H., and Tsodyks, M. (2002). Coding of Temporal Information by Activity-Dependent Synapses. *Journal of Neurophysiology*, 87(1):140–148.
- Hennig, M. H. (2013). Theoretical models of synaptic short term plasticity. *Frontiers in Computational Neuroscience*, 7(45).
- Karayannis, T., Elfant, D., Huerta-Ocampo, I., Teki, S., Scott, R. S., Rusakov, D. A., Jones, M. V., and Capogna, M. (2010). Slow GABA transient and receptor desensitization shape synaptic responses evoked by hippocampal neurogliaform cells. *The Journal of neuroscience*, 30(29):9898–909.
- Kohus, Z., Káli, S., Schlingloff, D., Papp, O., Rovira-Esteban, L., Freund, T. F., Hájos, N., and Gulyás, A. I. (2016). Properties and dynamics of inhibitory synaptic communication within the CA3 microcircuits of pyramidal cells and interneurons expressing parvalbumin or cholecystokinin. *The Journal of physiology*, 594(13):3745–74.
- Lee, S.-H., Földy, C., and Soltesz, I. (2010). Distinct endocannabinoid control of GABA release at perisomatic and dendritic synapses in the hippocampus. *The Journal of neuroscience*, 30(23):7993–8000.
- Loebel, A., Silberberg, G., Helbig, D., Markram, H., Tsodyks, M., and Richardson, M. J. E. (2009). Multiquantal release underlies the distribution of synaptic efficacies in the neocortex. *Frontiers in Cellular Neuroscience*, 3(27).
- Maass, W. and Markram, H. (2002). Synapses as dynamic memory buffers. *Neural Networks*, 15(2):155–161.
- Maccaferri, G., Roberts, J. D. B., Szucs, P., Cottingham, C. A., and Somogyi, P. (2000). Cell surface domain specific postsynaptic currents evoked by identified GABAergic neurones in rat hippocampus in vitro. *Journal of Physiology*, 524(1):91–116.
- Magee, J. C. and Cook, E. P. (2000). Somatic EPSP amplitude is independent of synapse location in hippocampal pyramidal neurons. *Nature neuroscience*, 3(9):895–903.
- Markram, H., Wang, Y., and Tsodyks, M. (1998). Differential signaling via the same axon of neocortical pyramidal neurons. *PNAS*, 95(9):5323–8.
- Markram, M., Muller, E., Ramaswamy, S., and Reimann, M. W. (2015). Reconstruction and Simulation of Neocortical Microcircuitry. *Cell*, 163:456–492.
- Migliore, R., Lupascu, C. A., Bologna, L. L., Romani, A., Courcol, J.-D., Antonel, S., Van Geit, W. A. H., Thomson, A. M., Mercer, A., Lange, S., Falck, J., Rössert, C. A., Shi, Y., Hagens, O., Pezzoli, M., Freund, T. F., Kali, S., Muller, E. B., Schürmann, F., Markram, H., and Migliore, M. (2018). The physiological variability of channel density in hippocampal CA1 pyramidal cells and interneurons explored using a unified data-driven modeling workflow. *PLoS Computational Biology*, 14(9):e1006423.
- Neu, A., Földy, C., and Soltesz, I. (2007). Postsynaptic origin of CB1-dependent tonic inhibition of GABA release at cholecystokinin-positive basket cell to pyramidal cell synapses in the CA1 region of the rat hippocampus. *The Journal of physiology*, 578(1):233–247.

- Pawelzik, H., Bannister, A. P., Deuchars, J., Ilia, M., and Thomson, A. M. (1999). Modulation of bistratified cell IPSPs and basket cell IPSPs by pentobarbitone sodium, diazepam and  $Zn^{2+}$ : Dual recordings in slices of adult rat hippocampus. *European Journal of Neuroscience*, 11(10):3552–3564.
- Pawelzik, H., Hughes, D. I., and Thomson, A. M. (2002). Physiological and morphological diversity of immunocytochemically defined parvalbumin- and cholecystokinin-positive interneurons in CA1 of the adult rat hippocampus. *Journal of Comparative Neurology*, 443(4):346–367.
- Pawelzik, H., Hughes, D. I., and Thomson, A. M. (2003). Modulation of inhibitory autapses and synapses on rat CA1 interneurons by GABAA receptor ligands. *Journal of Physiology*, 546(3):701–716.
- Price, C. J., Cauli, B., Kovács, E. R., Kukik, Á., Lambolez, B., Shigemoto, R., and Capogna, M. (2005). Neurogliaform Neurons Form a Novel Inhibitory Network in the Hippocampal CA1 Area. *Journal of Neuroscience*, 25(29):6775–6786.
- Price, C. J., Scott, R., Rusakov, D. A., and Capogna, M. (2008). GABAB Receptor Modulation of Feedforward Inhibition through Hippocampal Neurogliaform Cells. *The Journal of Neuroscience*, 28(27):6974–6982.
- Sik, A., Penttonen, M., Ylinen, A., and Buzsáki, G. (1995). Hippocampal CA1 Interneurons: An in vivo Intracellular Labeling Study. *Journal of Neuroscience*, 10(15):6651–6665.
- Thomson, A. M., Bannister, A. P., Hughes, D. I., and Pawelzik, H. (2000). Differential sensitivity to Zolpidem of IPSPs activated by morphologically identified CA1 interneurons in slices of rat hippocampus. *European Journal of Neuroscience*, 12(2):425–436.
- Tsodyks, M. and Markram, H. (1997). The neural code between neocortical pyramidal neurons depends on neurotransmitter release probability. *PNAS*, 94:719–723.
- Tsodyks, M., Uziel, A., and Markram, H. (2000). Synchrony generation in recurrent networks with frequency-dependent synapses. *The Journal of neuroscience*, 20(RC50).
- Vida, I., Halasy, K., Szinyei, C., Somogyi, P., and Buhl, E. H. (1998). Unitary IPSPs evoked by interneurons at the stratum radiatum — stratum lacunosum-moleculare border in the CA1. *Journal of Physiology*, 506(3):755–773.